CHARLES UNIVERSITY
Faculty of mathematics
and physics

Tides in terrestrial planets and icy moons

Marie Běhounková

Habilitation thesis

Department of Geophysics

Field: Geophysics

Prague 2021

To Jan and Jan

Contents

Preface **vii**

1 Introduction **1**
1.1 Impact of tides on planetary evolution 2
1.2 Tidal constraints on interior structure 5

2 Methods and models **7**
2.1 Tidal potential and response 7
2.2 Rheology 10
2.3 Tidal deformation 12
2.3.1 Normal mode theory 13
2.3.2 Solution in time domain 13
2.3.3 Tidal dissipation 17
2.4 Heat transfer 17
2.5 Orbital and rotational evolution 19
2.6 Coupling 20
2.7 Summary 21
2.8 List of symbols, definitions 25

3 Applications **29**
3.1 Susceptibility to tidal dissipation 29
3.2 Europa 31
3.3 Enceladus 33
3.4 Terrestrial exoplanets 39

4 Conclusions **43**

P Collection of publications **63**
Author's contribution to the publications 63
List of appended publications 63

P1 **Coupling mantle convection and tidal dissipation: Applications to Enceladus and Earth-like planets** **65**

P2 **Tidally induced thermal runaways on extrasolar Earths: Impact on habitability** **67**

P3 **Tidally-induced melting events as the origin of south-pole activity on Enceladus** **69**

P4 **Impact of tidal heating on the onset of convection in Enceladus's ice shell** **71**

P5 **Timing of water plume eruptions on Enceladus explained by interior viscosity structure** **73**

P6 **Effect of the tiger stripes on the deformation of Saturn's moon Enceladus** **75**

P7 **Tidal effects in differentiated viscoelastic bodies: a numerical approach** **77**

P8 **Plume Activity and Tidal Deformation on Enceladus Influenced by Faults and Variable Ice Shell Thickness** **79**

P9 **Tidal dissipation in Enceladus' uneven, fractured ice shell** **81**

P10 **Thermal and orbital evolution of low-mass exoplanets** **83**

P11 **Tidally-induced magmatic pulses on the oceanic floor of Jupiter's moon Europa** **85**

Preface

The tidal interaction has played an essential role in forming the Solar System as we know it. It contributed to shaping orbits, influencing the spin rate, and possibly capturing planetary bodies to spin-orbit resonances as observed for Mercury, Moon, and close-in satellites of giant planets. The unique volcanism on Jupiter's moon Io and the geysering activity at the south pole of Saturn's moon Enceladus furthermore point at tidal dissipation as an essential source of energy for some bodies of the Solar System. Tidal loading can also induce a strong internal stress field, causing unique geological patterns observed on Europa's young and tectonically modified surface. Tidal dissipation and tidal torque also link the orbital, rotational and thermal evolutions of planetary bodies leading to a complex problem on rich spectra of time scales and connecting geophysical and astronomical phenomena. This thesis consists of selected papers dedicated to the tidal deformation of planetary bodies with solid surfaces resulting in tidal dissipation and impacting internal evolution, rotational and orbital dynamics.

I started working on planetary-related topics and tidal deformation during my postdoctoral stay at the University of Nantes. Later, I have continued this cooperation at Charles University, and the work presented here benefits from it extensively. In particular, coupling the thermal and tidal evolution was initiated during my postdoctoral stay. Investigating the mutual feedback using the developed tools contributed to a better understanding of the susceptibility of terrestrial exoplanets and icy moons to tidal heating. Eventually, it inspired a broadening of applications to thermal-orbital-rotational evolution and investigating general aspects of the coupling. The tailored models for individual bodies helped interpret the results of past missions and assess possible measurable characteristics for future missions.

Here, I would like to acknowledge Ondřej Čadek for his insightful comments, suggestions and for triggering the cooperation with the University of Nantes. I have also benefited greatly from the close collaboration and discussions with Gael Choblet and Gabriel Tobie from the University of Nantes/CNRS and Ondřej Souček from Charles University. I also enjoyed working with my Ph.D. student Michaela Walterová Káňová. I greatly appreciate her for pushing boundaries towards astronomical applications. I would like to thank all the planetology group members, especially Klára Kalousová and Kateřina Pleiner Sládková, for the discussions. Among other collaborators, I would like to acknowledge (in alphabetical order) Mikael Beuthe,

Caroline Dumoulin, Jaroslav Hron, Mathilde Kervazo, Mohit Melwani Daswani, Francis Nimmo, Carolyn Porco, Christophe Sotin, and Steve Vance. I am also very grateful to Hana Čížková for her guidance at the beginning of my career. I want to thank Ladislav Hanyk for his flawless help with software and hardware support. I also am grateful to all the members of the Department of Geophysics. I acknowledge the support of the Czech Science Foundation (projects Nos. 19-10809S, 14-04145S, and P210/10/P306), Czech-French program BARRANDE, Ministry of Education of the Czech Republic (project Nos. MEB021129 and 8J20FR005), and computational resources of the IT4Innovations National Supercomputing Center, provided by The Ministry of Education, Youth and Sports from the Large Infrastructures for Research, Experimental Development and Innovations Project LM2015070 and LM2018140.

1 Introduction

A tide, raised on a body by its companion, results from the difference between the gravitational gradient across the finite-size object and the centrifugal forces due to its motion around the common barycenter. The way how the body reacts to tidal loading can impact its orbital, rotational and internal evolution. Tidal loading can occur on a wide range of frequencies. The static (non-periodic) part triggers a viscous flow in a body until a hydrostatic equilibrium is reached. The observed shape then reflects the density distribution and provides means to assess the internal structure of a body and the degree of its differentiation. Tidally-loaded bodies can also be subjected to periodic variations of the tidal force, which might result in significant periodic deformation and dissipation of mechanical energy. The periodic part of tidal loading occurs at frequencies too low for elastic response and too high to be described by a purely steady-state viscous creep. Viscoelastic, anelastic, and recently also empirical hereditary models are used to describe the body's reaction to tidal loading and a possible reaction lag. The amplitude of the response is mainly sensitive to the interior structure and rigidity, whereas the reaction lag and the amount of lost mechanical energy are controlled by its thermal state and rheological properties. Monitoring of induced periodic tidal deformation and gravity field can be instrumental in inferring the internal planetary characteristics. The associated tidal dissipation can result in a significant energy source for thermal evolution and leads to coupling between the tidal response and internal evolution. Tidal loading and the lagged response of the body can also lead to orbital evolution and despinning. As a result, tidal interaction couples the orbital-rotational-thermal evolution of planetary bodies. Recently, investigating the tidal deformation and the coupled orbital-rotational-thermal evolution has become attractive, especially in the context of planetary missions and the detection of exoplanets. Inspired by recent discoveries, this thesis is dedicated to (i) modeling tidally triggered processes and coupling the internal and tidal evolution of planetary bodies with solid surfaces in and beyond the Solar System and (ii) assessing the magnitude of tidal deformation and possible measurable characteristics.

1.1 Impact of tides on planetary evolution

Tidal loading, the lagged response of bodies, and the connected transfer of angular momentum and orbital energy can drive the long-term orbital and rotational evolution. Additionally, the resulting tidal dissipation can contribute significantly to the global energy budget, can be responsible for internal temperature increase, can even trigger the melting, and consequently can change the body's response to the tidal forcing.

The orbital evolution of the studied body is, in general, intertwined with the system's geometry and properties of its companion(s). In the simplest case, for a two-body system comprising a primary and a secondary (i.e., sun-planet or planet-moon), the dissipation of mechanical energy in the secondary drives the secondary to a lower orbit followed by an eccentricity decrease. In the systems of natural satellites, the orbital evolution is observed to be more complex. First, an orbiting secondary can raise tides on the primary. For a lagged response of the primary and for secondary on a prograde orbit, a resulting torque on the secondary below synchronous height can lead to a decrease of the semi-major axis and spiraling of the secondary towards its primary as observed for Phobos-Mars (Murray and Dermott, 1999). For a secondary above synchronous height, this effect results in an expansion of the orbit as observed for the Earth-Moon system (e.g., Wisdom and Tian, 2015) and contributes to the giant planets system evolution (e.g., Neveu and Rhoden, 2019). For a secondary without a companion, the outward motion also results in an eccentricity increase. However, orbit tends again to circularize as a consequence of the dissipation in the secondary.

For multi-bodies systems, the evolution is yet more complex as the tidal evolution can be influenced by the interaction between the bodies. The existence of mean motion resonances among the bodies have been suggested to maintain planets on eccentric orbits for relatively long periods (e.g., Dvorak et al., 2010). In such systems, tidal heating can also strongly fluctuate during the evolution of these bodies (e.g., Hussmann and Spohn, 2004), leading to episodes of high thermal activity in contrast to radiogenic heating, which progressively decays with time. Remarkably, the capture into mean-motion resonance may also result in the existence of equilibrium eccentricity and equilibrium heating as expected for Saturn's moon Enceladus. In this particular case, two competing processes are in equilibrium, i.e., circularization rate resulting from internal energy dissipation in the satellite and eccentricity growth in eccentricity-type mean motion resonance compensate each other. The total equilibrium heating rate in the satellite is, in this case, independent of the structure, and it is given by dissipation in the primary (e.g., Meyer and Wisdom,

2007).

Tidal torque acting on a body can also be responsible for its despining, capturing in a spin-orbit resonance, or pseudosynchronization (e.g., Makarov and Efroimsky, 2013; Correia et al., 2014; Ferraz-Mello, 2015; Walterová and Běhounková, 2020). The capture into synchronous orbit (1:1 spin-orbit resonance) is in the Solar System observed for the Moon and large moons of giant planets (e.g., see overview Hussmann et al., 2010). The higher-order resonances are theoretically predicted for bodies with large orbital eccentricities (e.g., Peale and Gold, 1965; Correia and Laskar, 2009; Ferraz-Mello, 2015). Within the boundaries of the Solar System, 3:2 spin-orbit resonance is observed for the planet Mercury. Also, for close-in exoplanets, the assumption of synchronous rotation is often used for low-eccentricity planets (cf. Walterová and Běhounková, 2020; Renaud et al., 2021). The capturing into spin-orbit resonance can also impact the thermal evolution. The body despins during the tidal locking and a significant amount of tidal heating may contribute to the thermal budget during the early stages of the evolution (see, e.g., Hussmann et al., 2010, for a summary). Additionally, tidally locked planets exhibit large surface temperature contrast between sub-stellar and anti-stellar sides due to uneven illumination of their surface if no atmosphere is present. This phenomenon is observed for Mercury, predicted (e.g., Dobrovolskis, 2013) and starting to be observed (e.g., Kreidberg et al., 2019) for close-in exoplanets and can impact the regime of the heat transfer (Summeren et al., 2011; Meier et al., 2021).

The missions to outer planets, especially Galileo to Jupiter's and Cassini-Huygens to Saturn's systems, pointed at tidal deformation and resulting heating as a mechanism influencing the internal processes in moons of outer planets. Effects originating in tidal flexing and heating are proposed to explain Io's volcanic activity. Tidal dissipation, together with radiogenic decay, governs the thermal evolution of Europa (e.g., Ojakangas and Stevenson, 1989; Hussmann et al., 2002; Tobie et al., 2003) and might shape Ganymede at the early stages of evolution (e.g., Showman et al., 1997; Bland et al., 2008). They are also responsible for the existence of past or present oceans in Enceladus, Dione, and Tethys (Neveu and Rhoden, 2019). Tidal effects also lie behind the existence of a very active province at Enceladus' south pole, the eruption of water vapors from warm ridges (e.g., Porco et al., 2006), and the huge total endogenic power (Howett et al., 2011; Spencer et al., 2018). Beyond the Solar system, tidal dissipation is also expected to affect the habitability of exoplanets (Barnes et al., 2008, 2009; Běhounková et al., 2011) and exomoons (Heller and Barnes, 2013; Dobos et al., 2017). It can also lead to thermal runaways and transform close-in terrestrial planets into lava worlds (Běhounková et al., 2011; Barr et al., 2018; Henning et al., 2018). The remote detectability of a large volcanic

activity around the closest stars could possibly confirm the tidally-induced activity (Kaltenegger et al., 2010).

The precise localization of dissipation in the terrestrial bodies and icy moons is still being discussed. For small moon Enceladus, the silicate core is possibly unconsolidated and porous due to low gravity, and consequently, it might be highly deformable and dissipative (Roberts, 2015; Choblet et al., 2017; Liao et al., 2020), explaining the observed ongoing hydrothermal activity (Hsu et al., 2015; Waite et al., 2017). On Jupiter's moon Io, the dissipation is connected to the silicate mantle, partially molten layer, or to a magma ocean (e.g., Tyler et al., 2015; Kervazo et al., 2021). On Europa, the deformation of the silicate mantle can also contribute to the heat budget, possibly prolonging volcanic activity until the present day (Běhounková et al., 2021). On icy satellites, the dissipation was also suggested to be connected to oceans (Tyler, 2014; Beuthe, 2016; Matsuyama et al., 2018; Wilson and Kerswell, 2018; Rovira-Navarro et al., 2019). However, the amount of dissipation is dampened if an elastic icy shell is present on top of the ocean (e.g., Beuthe, 2016; Matsuyama et al., 2018). Additionally, a significantly thinner ocean than may be expected from gravity and topography inversion is required to obtain a considerable contribution to the heat budget. Similarly, dissipation in the icy outer shell was suggested to be important (Tobie et al., 2005, 2008; Běhounková et al., 2012; Souček et al., 2019). Here, we concentrate on the dissipation in the solid parts of the bodies: ice shell of Enceladus, silicate mantles of Europa, and exoplanets.

Due to the sensitivity of rheological properties on the temperature, the tidal heating, and thermal evolution are coupled. The coupled thermal-orbital evolution has been investigated mainly for large satellites (e.g., Ojakangas and Stevenson, 1986; Fischer and Spohn, 1990; Hussmann and Spohn, 2004; Neveu and Rhoden, 2019) and for exoplanets (e.g., Shoji and Kurita, 2014; Driscoll and Barnes, 2015; Renaud et al., 2021). For exoplanets, partial melting was suggested to be a crucial regulating mechanism due to the large impact of the presence of melt on rheological properties leading to a decrease in tidal dissipation (Makarov et al., 2018). Partial melting can also be responsible for non-zero orbital eccentricities of exoplanets, for which the melt-free models predict fast circularization (e.g., Henning et al., 2009; Henning and Hurford, 2014; Makarov, 2015). For thermal-orbital-rotational evolution models, the thermal state proceeds as a sequence of thermal equilibria controlled by the spin-orbit resonance (Walterová and Běhounková, 2020).

Here, we focus on modeling of the positive feedback between the tidal dissipation and temperature increase leading to thermal runaways or melting. We studied the susceptibility of the ice shell of Enceladus and silicate mantles of Europa and exoplanets to tidal dissipation (chapter P1: Běhounková et al., 2010; chap-

ter P2: Běhounková et al., 2011; chapter P3: Běhounková et al., 2012; chapter P4: Běhounková et al., 2013; chapter P11: Běhounková et al., 2021). We have also investigated stable spin states characterized by zero tidal torque for empirically described rheology (chapter P7: Walterová and Běhounková, 2017; chapter P10: Walterová and Běhounková, 2020) and coupled orbital-rotational-thermal evolution of exoplanets with emerging magma oceans (chapter P10: Walterová and Běhounková, 2020).

1.2 Tidal constraints on interior structure

A body's response to tidal loading also plays an irreplaceable role in inferring the internal structure and allows for empirically assessing the link between tidal dissipation and viscosity. The static tides and rotation impacting the shape of the body can help determine the degree of differentiation and the radial density distribution assuming hydrostatic equilibrium. The information about the shape might be also essential for the characterization of close-in exoplanets in the future as the shape of observed transit light curves is suggested to be sensitive to the planet's triaxiality and can provide a constraint on the planetary structure (Akinsanmi et al., 2019; Hellard et al., 2019, 2020). Similarly, the additional gravitational potential induced by static tides directly affects the orbital apsidal precession on relatively short time scales. The first retrieval has been reported for Jupiter-like planet (Csizmadia et al., 2019), and it was suggested to be potentially detectable for terrestrial worlds under favorable conditions (Bolmont et al., 2020). Such measurement could supplement the mass and radius measurements and could reduce the degeneracy of the possible interior structures (e.g., Baumeister et al., 2020).

Monitoring the amplitude of periodic tidal deformation, induced gravitational potential, and phase lag between the loading and response from past or future spacecraft tracking (see Lainey, 2016, for a review) can also provide access to the interior structure and rheological parameters (e.g., van Hoolst et al., 2007; Dumoulin et al., 2017; Rivoldini et al., 2011; Khan et al., 2018; Kervazo et al., sub). For rocky and icy-rich exoplanets, it has been shown that induced gravitational potential is controlled by self-gravity and increases with the mass of the planet (Tobie et al., 2019). In some cases, tidal deformation and related phenomena can also be accompanied by body-specific features observable by spacecraft missions and hinting at conditions at the time of creation. For example, tidally induced stress could be responsible for producing lateral offset along Europa's strike-slip faults (Sládková et al., 2020), forming cycloids on Europa (e.g Rhoden et al., 2010) and faults at Enceladus' south pole (Rhoden et al., 2020). On Enceladus, the timing of observed geysering activity was suggested to be tidally driven (Hurford et al., 2007; Hedman

et al., 2013; Nimmo et al., 2014; Ingersoll et al., 2020) and possibly sensitive to the interior structure (Běhounková et al., 2015).

Here, we paid special attention to Saturn's moon Enceladus. We study the sensitivity of the observed geysering activity to the internal structure (chapter P5: Běhounková et al., 2015). In a tailored model, we have also studied the impact of variable ice shell thickness and prominent faults on the response of Enceladus' icy shell (chapter P6: Souček et al., 2016; chapter P8: Běhounková et al., 2017; chapter P9: Souček et al., 2019).

Methods and models 2

This chapter summarizes the description of tides, related phenomena and numerical treatment of tidal deformation used for applications in chapter 3. It compiles the individual models' components needed to evaluate the impact of tidal loading on the orbital-rotational evolution and the thermal evolution. The tidal potential acting on the secondary is described in section 2.1. The used constitutive laws describing the response of planetary bodies on the tidal periods are outlined in section 2.2. Section 2.3 summarizes the description of the tidal response and numerical approaches used for finding the solution. The method employed for the evaluation of the heat transfer is described in section 2.4. The secular evolutions of orbital parameters and spin rate used in the presented applications are briefly described in section 2.5. Section 2.6 summarizes the coupling schemes between the individual components. Table 2.1 compiles the method and approaches used in chapters P1–P11. The list of the used symbol is in section 2.8.

2.1 Tidal potential and response

Tidal force $\mathbf{f}^{\mathrm{tide}}$ acting on a perturbed body by a tide-rising perturber with mass m_* at distance r_* can be expressed in terms of tidal potential $\mathcal{U}^{\mathrm{tide}}$

$$\mathbf{f}^{\mathrm{tide}} = \nabla \mathcal{U}^{\mathrm{tide}}, \quad \mathcal{U}^{\mathrm{tide}} = \frac{\mathcal{G} m_*}{r_*} \sum_{l=2}^{\infty} \left(\frac{r}{r_*}\right)^l \mathcal{P}_l(\cos S_*), \tag{2.1}$$

where S_* is the angle from the perturber-perturbed body center axis, r is the radius of the perturbed body. See section 2.8 for the explanation of the remaining symbols. This potential can be expressed as a function of a point in the disturbed body (r, ϑ, φ). Kaula (1961, 1964) derived general decomposition of the tidal potential induced by an external point mass using the expansion in Keplerian elements $(a_*, e_*, i_*, \Omega_*, \omega_*, M_*)$ describing perturber apparent motion

$$\mathcal{U}^{\mathrm{tide}}(r, \vartheta, \varphi) = \sum_{l=2}^{\infty} \mathcal{U}_l^{\mathrm{tide}}(r, \vartheta, \varphi) = \sum_{l=2}^{\infty} \sum_{m=0}^{l} \sum_{p=0}^{l} \sum_{q=-\infty}^{\infty} \mathcal{U}_{lmpq}^{\mathrm{tide}}(r, \vartheta, \varphi). \tag{2.2}$$

where

$$\mathcal{U}^{\rm tide}_{lmpq}(r,\vartheta,\varphi) = \mathcal{B}_{lm}\mathcal{C}_{lmpq}r^l\mathcal{P}_{lm}(\cos\vartheta)\begin{Bmatrix}\cos\\ \sin\end{Bmatrix}^{l-m\ \text{even}}_{l-m\ \text{odd}}[v_{lmpq}-m(\varphi+\theta)], \tag{2.3}$$

$$\mathcal{B}_{lm} = \mathcal{G}m_*\frac{(l-m)!}{(l+m)!}(2-\delta_{0m}), \tag{2.4a}$$

$$\mathcal{C}_{lm} = \frac{1}{a_*^l}F_{lmp}(i_*)G_{lpq}(e_*), \tag{2.4b}$$

$$v_{lmpq} = (l-2p)\omega_* + (l-2p+q)M_* + m\Omega_* \tag{2.4c}$$

and θ is sidereal time (the rotation angle of the perturbed body). Note that inclination i_* can also be interpreted as obliquity β of the secondary relative to the orbit in our applications. Only degree $l = 2$ is usually taken in account due to low ratio $R_{\rm S}/a_*$. It has been, however, argued that higher degrees up to $l = 6$ are needed in the case of Phobos or very close asteroid binaries (Bills et al., 2005; Taylor and Margot, 2010). Here, we deal with moons/planets for which the use of degree $l = 2$ is sufficient, and special attention is paid to the tides raised by the primary (host star/planet) on the secondary (exoplanet/moon).

The expression $[v_{lmpq} - m(\varphi + \theta)]$ in eq. (2.3) can be further rewritten in terms of Fourier modes ω_{lmpq} (e.g., Efroimsky and Makarov, 2014)

$$v_{lmpq} - m(\varphi+\theta) = \omega_{lmpq}(t-t_0) - m\varphi + v_{lmpq}(t_0) - m\theta(t_0) \tag{2.5}$$

$$\omega_{lmpq} = (l-2p)\dot\omega_* + (l-2p+q)n + m(\dot\Omega_* - \dot\theta). \tag{2.6}$$

over which is the tidal potential expanded, and they correspond to frequencies of individual modes; n is the mean motion, t_0 the time of perigee passage.

In a particular case of bodies captured in 1:1 spin-orbit resonance ($n = \dot\theta$) and zero inclination, the leading term of the periodic part of tidal potential, eq. (2.2), can be written as

$$\begin{aligned}\mathcal{U}^{\rm tide} =& r^2n^2e\left(-\frac{3}{2}\mathcal{P}_{20}(\cos\vartheta)\cos nt + \right.\\ &\left.\frac{1}{4}\mathcal{P}_{22}(\cos\varphi)\,(3\cos nt\cos 2\varphi + 4\sin nt\sin 2\varphi)\right)\end{aligned} \tag{2.7}$$

for a body at periapse and x-axis pointing toward the primary at time $t = 0$. Interestingly, the leading term of the periodic part of the potential depends on e^1 for bodies in 1:1 spin-orbit resonance, whereas it is independent of the eccentricity for higher spin-orbit resonance.

In general, the body's response to the tidal potential can be computed for a body with a known structure and properties (section 2.3). It is, however, insightful and

conventional to wrap the tidal response by Love numbers (Love, 1907) to describe the tidal deformation for a radially symmetric body. Expressing deformation and induced potential as a single parameter can be especially helpful for monitoring tidal deformation of planetary bodies or for computations of the tidal evolution.

For an instant and linear response of a radially symmetric body, the potential Love number $k_\bullet$ expresses the induced potential $\delta\mathcal{U}^{\text{tide}}$ due to the mass transfer within the body relative to the loading potential $\mathcal{U}^{\text{tide}}$ at the surface $r = R_{\text{S}}$

$$\delta\mathcal{U}^{\text{tide}}(R_{\text{S}}, \vartheta, \varphi) = \sum_{l=2}^{\infty} \delta\mathcal{U}_l^{\text{tide}}(R_{\text{S}}, \vartheta, \varphi) = \sum_{l=2}^{\infty} k_l \mathcal{U}_l^{\text{tide}}(R_{\text{S}}, \vartheta, \varphi). \tag{2.8}$$

Similarly to potential Love number k_l, Love numbers h_l a l_l describe the tidally-induced surface deformation in radial (u_r) and lateral directions (u_ϑ and u_φ), (see, e.g., Burša and Pěč, 1988):

$$u_r(R_{\text{S}}, \vartheta, \varphi) \approx -\frac{1}{g} \sum_{l=2}^{\infty} h_l \mathcal{U}^{\text{tide}}(R_{\text{S}}, \vartheta, \varphi), \tag{2.9}$$

$$u_\vartheta(R_{\text{S}}, \vartheta, \varphi) \approx -\frac{1}{g} \sum_{l=2}^{\infty} l_l \frac{\partial \mathcal{U}^{\text{tide}}(R_{\text{S}}, \vartheta, \varphi)}{\partial \vartheta}, \tag{2.10}$$

$$u_\varphi(R_{\text{S}}, \vartheta, \varphi) \approx -\frac{1}{g} \sum_{l=2}^{\infty} l_l \frac{1}{\sin\vartheta} \frac{\partial \mathcal{U}^{\text{tide}}(R_{\text{S}}, \vartheta, \varphi)}{\partial \varphi}. \tag{2.11}$$

In eqs. (2.8–2.11), an instant response of the deformed body is assumed. However, the seismological and geodetic constraints on different time scales point at a delayed and frequency-dependent response and dissipation. In the above framework, the delay of the response to tidal loading can be included by complex Love numbers, tidal phase lag, or quality factor (dissipation function). The phase lag $\varepsilon_{lmpq} = \varepsilon(\omega_{lmpq})$ describes lagging between the induced and loading potentials for the lm harmonic and the pq Fourier mode. The complex potential Love number is defined using the phase lag and the potential Love number as follows

$$\widehat{k}_l(\omega_{lmpq}) = k_l \exp(-\mathrm{i}\varepsilon_{lmpq}). \tag{2.12}$$

In the tidal theory, the dissipation function (inverse quality factor) is related to the phase lag through (Efroimsky, 2012)

$$Q^{-1}_{lmpq} = \sin|\varepsilon_{lmpq}|\,. \tag{2.13}$$

The values of phase lag and dissipation are controlled by properties of the deformed body and can be inferred using constitution laws. Note, however, that individual modes can be coupled for aspherical bodies. However, the numerical models not requiring the assumption of the spherical symmetry can also lead to the evaluation of the Love numbers k_{lm}, h_{lm} and l_{lm} (see, e.g., Lainey, 2016, for a summary) and can be used to study a spectral coupling.

2.2 Rheology

For a general linear elastic and isotropic body, Hooke's elastic solid (e.g., Martinec, 2019)

$$\mathbf{s} = \lambda \mathrm{tr}(\mathbf{e}) + 2\mu\mathbf{e} \tag{2.14}$$

describes the constitutive relationship between the incremental Euler strain tensor $\mathbf{e} = \frac{1}{3}\mathrm{tr}(\mathbf{e})\mathbf{I} + \mathbf{e}'$ and the Cauchy stress tensor $\mathbf{s} = \frac{1}{3}\mathrm{tr}(\mathbf{s})\mathbf{I} + \mathbf{s}' = -p\mathbf{I} + \mathbf{s}'$ and λ and μ denote the Lamé parameters. Separating the strain and stress tensor into the isotropic and deviatoric parts the Hooke's law splits into

$$-p = K\mathrm{tr}(\mathbf{e}), \quad K = \lambda + \frac{2}{3}\mu \tag{2.15a}$$

$$\mathbf{s}' = 2\mu\mathbf{e}'. \tag{2.15b}$$

The isotropic part in the planetary applications is usually considered elastic with a few notable exceptions (Beuthe, 2013; Kervazo et al., 2021). For the deviatoric part, viscoelastic or anelastic behavior is taken into account to comply with the observed dissipation and phase lag constraints in planetary bodies.

In the linear theory abandoning purely elastic behavior, the compliance operator $\overline{J}$ is used to map the current and past stress on the value of the strain (e.g., Efroimsky, 2012)

$$2\mathbf{e}' = \overline{J}(t)\mathbf{s}' = \int_{-\infty}^{t} J(t-t')\dot{\mathbf{s}}'(t')\mathrm{d}t', \tag{2.16}$$

$J(t-t')$ denotes the compliance function or the creep-response function. In the frequency domain, after invoking the correspondence principle and applying the Fourier transform, the above relationship yields

$$2\widehat{\mathbf{e}'}(\omega) = \widehat{J}(\omega)\widehat{\mathbf{s}'}(\omega), \tag{2.17}$$

where $\widehat{\bullet}$ corresponds to the image in the frequency domain and $\widehat{J} = i\omega\int_0^\infty J(\tau)e^{-i\omega\tau}\mathrm{d}\tau$ (Jackson, 2015) is the complex compliance. Similarly, defining the complex rigidity

$$\widehat{\mu}(\omega) = 1/\widehat{J} \tag{2.18a}$$

leads to the analogy of Hooke's law in the frequency domain

$$\widehat{\mathbf{s}'} = 2\widehat{\mu}\widehat{\mathbf{e}'}. \tag{2.18b}$$

An overview of often considered viscoelastic/anelastic rheologies is given in, e.g., Renaud and Henning (2018). Here, only the rheologies used in chapters P1 to P11 are

summarized. Due to historical reasons, applicability in some cases, and simplicity, the Maxwell rheology is used (Běhounková et al., 2010, 2012). The compliance for the Maxwell rheology reads (e.g., Efroimsky, 2012)

$$J_{\mathrm{M}}(t-t') = \frac{1}{\mu}\left(1+\frac{t-t'}{\tau_{\mathrm{M}}}\right)\Theta(t-t') \qquad \text{in time domain} \tag{2.19a}$$

$$\widehat{J}_{\mathrm{M}}(\omega) = \frac{1}{\mu}\left(1-\frac{\mathrm{i}}{\omega\tau_{\mathrm{M}}}\right) \qquad \text{in frequency domain;} \tag{2.19b}$$

$\tau_{\mathrm{M}} = \eta/\mu$ is the Maxwell time, η is the viscosity and Θ denotes the Heaviside step function. Nevertheless, the Maxwell rheology underestimates the dissipation rate for forcing periods shorter than the Maxwell time. Consistent with the available empirical constraints on the link between tidal dissipation function and viscosity (e.g Tobie et al., 2019; Samuel et al., 2019) the Andrade rheology is recently used (e.g., Efroimsky and Lainey, 2007; Běhounková et al., 2015; Walterová and Běhounková, 2017, 2020). The compliance for the Andrade rheology (Efroimsky, 2012) is given by

$$J_{\mathrm{A}}(t-t') = \frac{1}{\mu}\left(1+\left(\frac{t-t'}{\zeta_{\mathrm{A}}\tau_{\mathrm{M}}}\right)^{\alpha_{\mathrm{A}}}+\frac{t-t'}{\tau_{\mathrm{M}}}\right)\Theta(t-t') \qquad \text{in time domain} \tag{2.20a}$$

$$\widehat{J}_{\mathrm{A}}(\omega) = \frac{1}{\mu}\left(1+(\mathrm{i}\omega\zeta_{\mathrm{A}}\tau_{\mathrm{M}})^{-\alpha_{\mathrm{A}}}\,\Gamma(1+\alpha_{\mathrm{A}})-\frac{\mathrm{i}}{\omega\tau_{\mathrm{M}}}\right) \qquad \text{in frequency domain.} \tag{2.20b}$$

The Andrade rheology describes well the body's response from the instant elastic deformation through transient creep important for tidal deformation to viscous flow. Microscopic processes underlying empirical Andrade model are discussed in, e.g., Sundberg and Cooper (2010). Conveniently for numerical computations, the Andrade rheology depends on only two additional parameters, α_{A}, and ζ_{A}, compared to the Maxwell rheology. The Andrade parameter α_{A} is expected to vary between 0.1 and 0.4 (Gribb and Cooper, 1998; Jackson et al., 2002; Castillo-Rogez et al., 2011). For methods solving the tidal deformation in the time domain, the rheologies with a transient creep might not be, however, easy to reconcile with due to numerical considerations. The effective viscosity can be designed to compensate for the underestimation of the dissipation rate for the Maxwell rheology for a single frequency forcing. The effective viscosity η_{eff} is defined based on the observed dissipation function (Běhounková et al., 2010, 2011) or consistent with mechanical tests showing that the effective viscosity during transient creep is smaller than viscosity during steady-state creep (Běhounková et al., 2012). Optionally, the effective viscosity η_{eff} mimicking the Andrade rheology characteristics (i.e., Andrade-like rheology) has been proposed (Běhounková et al., 2013; Souček et al., 2019; Běhounková et al., 2021).

2.3 Tidal deformation

Computing tidal deformation belongs among traditional problems in planetary science. Several theoretical approaches and numerical models have been developed to evaluate tidal deformation. Approaches based on the normal mode theory are widely used to compute tidal deformation and other processes on various time scales, including post-glacial rebound, Chandler wobble, seismic, and normal modes applications (e.g., Takeuchi and Saito, 1972; Wu and Peltier, 1982; Sabadini and Vermeersen, 2004; Tobie et al., 2005; Wahr et al., 2009; Jara-Orué and Vermeersen, 2011; Kervazo et al., 2021). The implementations evaluating tidal deformation are formulated in the frequency domain, various linear rheological descriptions are easily included. Additionally, they are fast and describe the deformation of the whole body. On the other hand, the undeformed body (layer and rheological parameters) must be radially symmetric.

For bodies with thin shells above subsurface oceans (e.g., Europa, Enceladus), the outer ice shell can be approximated by a membrane around a fluid layer, and it can be modeled as a viscoelastic membrane (Beuthe, 2015a,b) for which variations of the ice shell may be introduced (Beuthe, 2018, 2019). This approach is fast and different rheologies can also be readily included.

Evaluating a solution in the time domain was proposed by Tobie et al. (2008) to investigate the effects of laterally variable viscosity in a spherical shell. The impact of variable viscosity can be important if coupled with thermal evolution (Běhounková et al., 2010). Even more detailed models of tidal deformation can be tailored to describe individual bodies in detail and to comply with observed properties. In general, these models are usually the most time and memory demanding and are based on the finite element method (A et al., 2014; Souček et al., 2016; Běhounková et al., 2017; Souček et al., 2019; Steinke et al., 2020).

In chapters P1 to P11, an approach employing classical normal mode theory as well as the solution in time domain based on combined finite-difference/spherical-harmonic or finite elements method are used. The choice of the method depends on the needs of individual applications (see also table 2.1). The use of various methods is also irreplaceable in investigating the methods' assumptions on resulting deformation and for benchmarking (Běhounková et al., 2018). A short overview of the methods is given below. The derivation can be found in specialized literature (e.g, Sabadini and Vermeersen, 2004; Souček et al., 2019).

2.3.1 Normal mode theory

The normal mode theory (NMT) is a classical method of solving tidal deformation in the whole body. We, therefore, restrict ourselves here to a brief description of basic principles. The detailed derivations are given in, e.g., Sabadini and Vermeersen (2004). NMT solves mass, momentum conservations, and Poisson equation supplemented by the constitutive law. It employs the spherical harmonic expansion in the space domain and the Fourier transformation into the frequency domain. The spheroidal solution for a unit load can be then rewritten into a set of ordinary differential equations, for vector $\mathbf{y}_l(r)$, where its components represent radially dependent functions describing the radial and tangential displacements, the radial and tangential stress, the gravitational potential, and the gravitational potential stress in the frequency domain, respectively. The approach based on the propagation matrix technique is used to find the solution in the radial direction. The solution is computed in the entire spherically symmetric body, and it is constrained by boundary conditions corresponding to the free surface at the top and regularity in the center. Using NMT, Love numbers at the surface, R_S, can be very easily computed as (Matsuyama et al., 2018)

$$k_l(\omega) = -(\mathbf{y}_l)_5(R_\mathrm{S}, \omega) - 1 \tag{2.21a}$$

$$h_l(\omega) = g(R_\mathrm{S})(\mathbf{y}_l)_1(R_\mathrm{S}, \omega) \tag{2.21b}$$

$$l_l(\omega) = g(R_\mathrm{S})(\mathbf{y}_l)_2(R_\mathrm{S}, \omega), \tag{2.21c}$$

where $(\mathbf{y}_l)_i$ is the i-th component of the spheroidal solution vector for degree l. Moreover, the solution $\mathbf{y}_l$ obtained by NMT is, in general, complex as the constitutive law is described by the analogy of Hooke's law in the frequency domain eq. (2.18b). Different rheologies can be, therefore, without difficulty included by changing values of the complex rigidity. Additionally, the complex solution contains information about the amplitude of deformation and stresses and their lagging. These properties combined with the relative simplicity of the NMT based method make computational tools working in the frequency domain universally used for evaluating the tidal deformation (e.g., Wahr et al., 2009). However, the approaches based on NMT cannot easily include lateral variations of rheological properties or non-spherical boundaries.

2.3.2 Solution in time domain

Approaches in this section aim to describe the tidal deformation in bodies with 3D variations of rheological parameters and aspherical surfaces. We use formulation in the time domain, and we employ the Eulerian approach. Furthermore, we solve tidal deformation only in solid parts, typically an outer ice shell. The impact of other

parts is neglected or parameterized. Both an incompressible (FD-SH method) and a compressible (FE method) bodies are considered.

The time-varying tidal potential $\mathcal{U}^{\text{tide}}$ generates additional stress (incremental Cauchy stress) $\mathbf{s}$ and displacement $\mathbf{u}$. For the current configuration and considering a small deformation and compressible body, the density of the deformed body is described as

$$\rho(\mathbf{r}) = \rho_0 \left(1 - \nabla \cdot \mathbf{u}(\mathbf{r})\right), \tag{2.22a}$$

where ρ_0 is the reference density. It furthermore holds

$$\nabla \cdot \mathbf{u}(\mathbf{r}) = 0, \tag{2.22b}$$

if we investigate the deformation of an incompressible body. The momentum equation for the incremental Cauchy stress tensor $\mathbf{s}$ follows

$$\nabla \cdot \mathbf{s} + \rho_0 \nabla \mathcal{U}^{\text{tide}} + \rho_0 \nabla \delta\mathcal{U}^{\text{tide}} = \mathbf{0}, \tag{2.23}$$

where the volume changes due to the deformation and the inertial force are neglected. The incremental gravitational potential $\delta\mathcal{U}^{\text{tide}}$ due to deformation, i.e., self-gravity term, is induced only by boundaries deformation, and it is computed using the properties of the gravitational potential and the condensation method (Martinec et al., 1993).

At the deformed surface, the free surface conditions hold. In the approaches presented here, we prescribe the boundary conditions on the undeformed body. Using a Taylor series to the first order in $\mathbf{u}$, the boundary condition on the undeformed body follows

$$\mathbf{s} \cdot \mathbf{n}_{\text{S}} + u_r \rho_0 g \mathbf{n}_{\text{S}} = 0, \tag{2.24}$$

where $\mathbf{n}_{\text{S}}$ is the outer normal to the undeformed surface; note that these conditions can also be interpreted as a force equilibrium. The above equation also includes the assumption that the pre-stress is dominated by the hydrostatic pressure p_0. Other possible components, such as contributions due to viscous flow, are small in comparison. As the approach in the time domain solves the deformation only in part of the body, the boundary conditions at the bottom have to be added to constrain the solution. Compared to the surface, the pressure in the liquid layer below induced by the loading and additional potential has to be considered

$$\mathbf{s} \cdot \mathbf{n}_{\text{B}} - u_r(\rho_{\text{ll}} - \rho_0) g \mathbf{n}_{\text{B}} = -\mathbf{n}_{\text{B}} \rho_{\text{ll}} (\mathcal{U}^{\text{tide}} + \delta\mathcal{U}^{\text{tide}}), \tag{2.25}$$

where ρ_{ll} is the density of the underlying liquid layer and $\mathbf{n}_{\text{B}}$ is the outer normal to the undeformed bottom boundary.

Two methods of solving the above equations supplemented by the rheological law (section 2.2) are used. Similar to NMT, the first method employs spherical harmonics expansion in the lateral direction and takes advantage of the problem separated by degree for only depth-dependent rigidity. The second method is based on the finite element method allowing for variable shell thickness, viscosity, and rigidity. This approach, however, leads to a computationally challenging problem. Compared to the NMT solved in the frequency domain, the time discretization scheme for a non-elastic case has to be considered.

Finite difference-spherical harmonic decomposition method (FD-SH method) solves the equations describing a tidal deformation in a spherical shell with radially symmetric shear modulus and general (3D dependent) viscosity (Tobie et al., 2008; Běhounková et al., 2010; Běhounková et al., 2015). It takes into account the incompressible body and allows for including the Maxwell and the Andrade rheologies. The Andrade rheology in the time domain (eq. (2.20a)) can be rewritten

$$2\mathbf{e}' - \frac{\mathbf{s}'}{\mu} = \int_0^t \frac{\mathbf{s}'(t')}{\eta}\mathrm{d}t' + \int_0^t \mu^{\alpha_\mathrm{A}-1}\frac{(t-t')^{\alpha_\mathrm{A}}}{(\zeta_\mathrm{A}\eta)^{\alpha_\mathrm{A}}}\dot{\mathbf{s}}'(t')\mathrm{d}t', \tag{2.26}$$

assuming stress-free initial conditions ($\mathbf{s}(t<0)=\mathbf{0}$). It is discretized in time for $i+1$-th time step as follows

$$2\mathbf{e}'_{i+1} - \frac{\mathbf{s}'_{i+1}}{\mu} = \sum_{j=0}^{i}\frac{\mathbf{s}'_j}{\eta}\Delta t + \sum_{j=0}^{i-1} w_{ij}\frac{\mathbf{s}'_{j+1}-\mathbf{s}'_{j-1}}{(\zeta_\mathrm{A}\eta)^{\alpha_\mathrm{A}}} \tag{2.27}$$

where Δt is the constant time step and $w_{ij} = \frac{1}{2}(i-j+1)^{\alpha_\mathrm{A}}\Delta t^{\alpha_\mathrm{A}}\mu^{\alpha_\mathrm{A}-1}$ is the weight factor. Viscosity is assumed to be constant through one tidal period. The Maxwell rheology is treated analogically, and the last term on the RHS is omitted.

In lateral directions, decomposition in the spherical harmonics (Varshalovich et al., 1988) allows rewriting eqs. (2.22b), (2.23–2.25) and (2.27) as a set of ordinary differential equations for spherical harmonic coefficients of stress and displacement components. In the case of the shear modulus only radially dependent and the memory term (RHS of eq. (2.27)) included explicitly, the system further separates into spheroidal and toroidal parts for a given degree j (analogically to NMT method), and only right-hand side depends on order $m = 0, \ldots, j$. Therefore, determining the solution is not strenuous up to $j \approx 100$ as it has to be evaluated only for a given j and then applied to all RHS. In the radial direction, staggered finite difference method (Gerya, 2010) is employed for solving the ordinary differential equation system.

Spherical harmonic decomposition is advantageous and natural for expressing the self-gravity potential $\delta\mathcal{U}^{\mathrm{tide}}$ originating in the boundaries deformation. The

difficulty for this method lies in the expressing terms containing $\mathbf{s}(\mathbf{r})/\eta(\mathbf{r})$ due to the multiplication of two series in spherical harmonic formalism. Abandoning the use of an analytic formula (Varshalovich et al., 1988) due to its inefficiency, the problematic term is computed numerically using tensor-scalar multiplication on a grid (Martinec, 1989) and making use of Gauss-Legendre quadrature formula in latitudinal direction and fast Fourier transform in the longitudinal direction (Press et al., 1992). Moreover, the computation of this multiplication is layer-based and can be easily parallelized using MPI.

Finite element method (FE) A disadvantage of the FD-SH method is the inclusion of lateral variations only for the viscosity, while the shape and shear modulus μ has to be spherically symmetric to exploit the computational efficiency. These models might not be sufficient for some bodies in the Solar System, such as Enceladus (e.g., Souček et al., 2016) and this disadvantage can be eliminated by the use of the finite element method. In this approach, compressibility is included. The elastic rheology (eq. (2.15a)) is considered for the isotropic part. Due to numerical reasons, a Maxwell model is used, and the time derivative of the Maxwell rheology is considered

$$\dot{\mathbf{s}'} = 2\mu\dot{\mathbf{e}'} - \frac{\mu}{\eta}\mathbf{s}' \tag{2.28}$$

to express the constitutive law. Again, the explicit time discretization with a constant time step Δt is employed, for the $i+1$-th time holds

$$\mathbf{s}^{i+1} = K\mathrm{tr}(\mathbf{e})\mathbf{I} + \frac{2\mu}{1+\Delta t/\tau_{\mathrm{M}}}((\mathbf{e}')^{i+1} - (\mathbf{e}')^{i}) + \frac{1}{1+\Delta t/\tau_{\mathrm{M}}}(\mathbf{s}')^{i}\,. \tag{2.29}$$

Besides the boundary conditions, zero displacement of the center of the figure and zero net-body rotation have to be added to constrain the quasi-static formulation, and these additional conditions are implemented using Lagrange multipliers. Additional induced potential $\delta\mathcal{U}^{\mathrm{tide}}$ originating in the boundaries deformation is considered. It is computed using the spherical harmonic expansion of the surface displacement, followed by the same procedure as for the FD-SH method. The weak formulation and the space discretization by the Galerkin method are described in Souček et al. (2016) and Souček et al. (2019) in detail. This method is implemented using the available building blocks provided by FEniCS (Alnaes et al., 2015) and PETSc libraries are used, ensuring a good parallel performance. Due to the presence of Lagrange multipliers in the boundary value problem and associated loss of positive-definiteness, the present-day implementation is restricted to the use of direct solvers. The disadvantage of this method is the large memory and time demands.

Periodic solution Using the approaches above, we search for a periodic solution independent of the initial conditions. The time integration for both methods solved in the time domain is, therefore, performed until a converged solution of the viscoelastic/anelastic problem is reached, i.e., when the differences in deformation or dissipation rate are sufficiently small between times t and $t + P$ (see Běhounková et al., 2010, for more details). The solution is integrated from an undeformed state ($\mathbf{u}(t = 0) = \mathbf{0}$), and finding the converged solution can be time-consuming.

2.3.3 Tidal dissipation

The periodic tidal deformation can also directly impact the heat budget and thermal evolution due to the dissipation of the mechanical energy. The tidal dissipation rate has to be evaluated locally to investigate its impact on temperature evolution. The local volumetric tidal heating dissipation averaged through one forcing period P is given by

$$h_{\mathrm{tide}}(\mathbf{r}) = \frac{1}{P}\int_t^{t+P} \mathbf{s}(\mathbf{r}, t') : \dot{\mathbf{e}}(\mathbf{r}, t')\mathrm{d}t', \tag{2.30}$$

where $\mathbf{s}$ and $\dot{\mathbf{e}}$ are computed using the methods described in section 2.3. Its integration over the body is usually called global dissipation P_{tide}. Again, it is also insightful to evaluate the global dissipation in the body for general tidal potential using the Love numbers (Efroimsky and Makarov, 2014; Walterová, 2021):

$$\begin{aligned} P_{\mathrm{tide}} = -\frac{\mathcal{G}m_*^2}{a}\sum_{lmpq}\left(\frac{R_{\mathrm{S}}}{a}\right)^{2l+1} (2-\delta_{m0})\,\frac{(l-m)!}{(l+m)!}\times \\ \times\,(G_{lpq}(e_*))^2\;(F_{lmp}(i_*))^2\;\omega_{lmpq}\,\mathrm{Im}\left(\widehat{k}_l(\omega_{lmpq})\right). \end{aligned} \tag{2.31}$$

Inspection of this formula shows that the contribution of zero-frequency (static) contribution to the global heat budget is zero as expected. For a body in 1:1 spin-orbit resonance and zero inclination (see also section 2.1), the leading term of tidal heating depends on eccentricity as e^2 and the tidal heating in this resonance is, therefore, sensitive to eccentricity changes. On the other hand, the leading term is e^0 for bodies captured in higher spin-orbit resonances, and dissipation is only weakly sensitive to the eccentricity changes.

2.4 Heat transfer

Periodic tidal deformation can also affect the long-period thermal evolution via tidal dissipation, and it should be included as a heat source of the thermal evolution. The widely used Boussinesq (BA) or extended Boussinesq (EBA) approximation (e.g.,

King et al., 2010) is here solved to describe the thermal evolution. The mass, momentum, and energy conservation and constitutive equations for in the extended Boussinesq approximation[1] read (see section 2.8 for the overview of the used symbols)

$$\nabla \cdot \mathbf{v} = \mathbf{0}, \tag{2.32a}$$

$$-\nabla\pi + \nabla \cdot \boldsymbol{\sigma}' - \alpha \left(T - \bar{T}(r)\right) \rho_0 \mathbf{g}(r) = \mathbf{0} \tag{2.32b}$$

$$\rho_0 c_\mathrm{p} \frac{\partial T}{\partial t} = k\nabla^2 T - \rho_0 c_\mathrm{p} \mathbf{v} \cdot \nabla T + \rho_0 \alpha T \mathbf{v} \cdot \mathbf{g}(r) + \boldsymbol{\sigma}' : \nabla \mathbf{v} + \\ + h_\mathrm{rad} + h_\mathrm{tide} - h_\mathrm{melt}, \tag{2.32c}$$

$$\boldsymbol{\sigma}' = \eta(T) \left(\nabla \mathbf{v} + (\nabla \mathbf{v})^\mathrm{T}\right). \tag{2.32d}$$

Compared to periodic tidal deformation, the heat transfer takes place on a longer time scale and, therefore, viscous flow is considered. Free-slip and temperature boundary conditions are mostly prescribed (cf. table 2.1) to constrain the solution of the above equations.

The temperature dependence of rheological parameters is essential as it couples the long-term thermal evolution and tidal deformation on the shorter periods resulting in tidal dissipation. The temperature dependence of the viscosity is described by Arrhenius law (Běhounková et al., 2013; Běhounková et al., 2012; Walterová and Běhounková, 2020; Běhounková et al., 2021) or Frank-Kamenetskii approximation (Běhounková et al., 2010, 2011). In Běhounková et al. (2013), the composite rheology accounting for observed deformation mechanisms was additionally included (Goldsby and Kohlstedt, 2001).

A special attention is paid to the volumetric heat sources (eq. (2.32c)) originating in tidal dissipation as described in section 2.3.3. For silicate mantles, radiogenic heating is considered as another important source of energy (Běhounková et al., 2011, 2021). Furthermore, the temperature can reach the solidus temperature for large values of internal dissipation and non-effective heat transfer. A simple model of instantaneous melt extraction is introduced. It is triggered for the temperature at the melting point and ensures that the solidus temperature is not exceeded, i.e., h_melt represents an energy sink and it is determined iteratively. The model also assumes that the energy excess is consumed by melting through latent heating, and the melt is immediately transported to the boundary.

From the technical point of view, we solve eqs. (2.32a–2.32d) in a spherical shell. The numerical treatment is described in Choblet (2005) and Choblet et al. (2007). The method is based on the composite mesh using the "cubed sphere" transformation

[1] For BA, the third and fourth terms on RHS in eq. (2.32c) are neglected.

dividing spherical shell into six equivalent blocks (Ronchi et al., 1996). The numerical solution employs the finite volume method. The Stokes problem eqs. (2.32a) and (2.32b) is solved using the FAS/multigrid method, V cycles, and Gauss-Seidel smoother. Linear transfer operators are considered except for the pressure. Prolongation of pressure is based on Tackley (2008) for better treatment of large viscosity gradients. The energy conservation eq. (2.32c) uses the Godunov-like method for the advective term. Courant criterion controls the time step.

The solution in the 3D domain is usually time-consuming, especially if many models have to be evaluated. For planetary applications, the heat transfer is therefore frequently described by 1D parameterization employing scaling laws (e.g., Solomatov, 1995). This approach based on Tosi et al. (2017) was adapted in Walterová and Běhounková (2020).

2.5 Orbital and rotational evolution

Besides the impact on the thermal evolution, the tidal loading of deformable bodies raises additional potential. Neglecting other possible sources, the additional potential due to the planet's deformation represents a perturbation to the two-body problem. The theory used to compute the orbital elements' evolution usually accounts for the description of bodies based on or analogical to Love numbers as described above. In this linear theory (Kaula, 1961) and employing the Love numbers, the additional potential can be rewritten into the Fourier modes of disturbing function and used in Lagrange planetary equations. The secular evolution of the semi-major axis and eccentricity due to the secondary's deformation then leads to (Walterová and Běhounková, 2020)

$$\dot{a} = -\sum_{lmpq} \frac{2\mathcal{G}m_*}{na} \frac{R_\mathrm{S}^{2l+1}}{a^{2l+2}} (l-2p+q)\times \\ \times \frac{(l-m)!}{(l+m)!}(2-\delta_{0m})\ (G_{lpq}(e))^2\ (F_{lmp}(i))^2\ k_l\ \sin\varepsilon_{lmpq} \tag{2.33a}$$

$$\dot{e} = -\sum_{lmpq} \frac{\mathcal{G}m_*}{na^2} \frac{\sqrt{1-e^2}}{e} \frac{R_\mathrm{S}^{2l+1}}{a^{2l+2}} \left(\sqrt{1-e^2}(l-2p+q)-(l-2p)\right)\times \\ \times \frac{(l-m)!}{(l+m)!}(2-\delta_{0m})\,(G_{lpq}(e))^2\ (F_{lmp}(i))^2\ k_l\ \sin\varepsilon_{lmpq}\,. \tag{2.33b}$$

Again, the inclination i_* is here equal to the obliquity β, and it is set to zero for applications in Walterová and Běhounková (2020).

The gravitational force acting on the unaligned tidal bulge also results in tidal torque influencing the secondary's spin state. The secular tidal evolution of the

secondary's spin rate is computed from (e.g, Efroimsky and Williams, 2009)

$$C\ddot{\theta} = \mathcal{T}, \tag{2.34a}$$

where C is the principal moment of inertia. Analogically to the disturbing function, the secular torque's component orthogonal to the planetary equator $\mathcal{T}$ (e.g., Efroimsky and Williams, 2009; Walterová and Běhounková, 2020) can be rewritten in terms of Fourier modes

$$\mathcal{T} = \frac{\mathcal{G}m_*^2}{a} \sum_{lmpq} \left(\frac{R_\mathrm{S}}{a}\right)^{2l+1} \frac{(l-m)!}{(l+m)!} (2-\delta_{0m})\, m\, \left(G_{lpq}(e)\right)^2\, \left(F_{lmp}(i)\right)^2\, k_l\, \sin\varepsilon_{lmpq}\,. \tag{2.34b}$$

The integration of the above equations make use of the fourth-order predictor-corrector scheme (Hamming's method, Ralston, 1965).

For the sake of completeness, we emphasize that the equations in this section consider only the disturbing potential due to the secondary's deformation, and they are considered in Walterová and Běhounková (2020). As discussed in chapter 1, the processes in systems of natural satellites are more complex. We rely in our applications on parameterized evolution (Běhounková et al., 2021) or discussion of the total equilibrium energy rate (Běhounková et al., 2012; Běhounková et al., 2017; Souček et al., 2019).

2.6 Coupling

Determining the time evolution of moons and terrestrial planets requires a description of processes of different time scales. The tidal time-scale is on time scales from hours to months. Depending on the tidal dissipation rate, the secular despining of bodies at the beginning of the evolution can span on time scales from thousands of years. Mantle/ice shell convection operates on the time scale of thousands to hundreds of millions of years. The eccentricity and the semi-major axis secular evolutions operate on the time scale from hundreds of millions of years, again depending on the system configuration[2]. The problem must be simplified, and several assumptions must be made to evaluate the coupled evolution numerically. Typically, it is assumed that the stress induced by processes on various periods does not mutually interact with each other, and pre-stress is dominated by hydrostatic pressure (section 2.3), and only time average characteristics of short-period processes impact the processes describing the long-term evolution while the long-term characteristics are taken as a constant on short-time scales.

[2]Note evolution of a planet without a companion is considered here (section 2.5)

Special attention here is paid to susceptibility of thermal evolution to tidal heating (see chapters P1 to P4 and P11) assuming constant or parameterized orbital and rotational parameters. The tidal dissipation rate, averaged over one tidal period and employing the 3D temperature field determined by the convective flow (section 2.3), is imposed as a source of volumetric heating for heat flow (section 2.4). Due to the temperature dependence of rheological parameters on temperature, the tidal dissipation is repeatedly updated using the finite difference/spherical harmonic approach. Typically, the tidal dissipation has to be updated after a few tens of convection time steps (Běhounková et al., 2010).

Taking into account also orbital and rotational evolution leads to a more complex time scheme. We concentrate on first-order effects. 1D parameterization of convection and method based on NMT are, therefore, used. The following time scheme is adopted in Walterová and Běhounková (2020). First, during the initial despinning period, the spin rate, as well as the semi-major axis, the eccentricities, and interior, are evolving until a stable spin is found. After this initial period, the time step in the long-period cycle is taken, during which the eccentricity, semi-major axis, and interior temperature evolve while the spin rate is considered constant. After each long-period time step, the new equilibrium of the spin state is found assuming constant orbital parameters. As the interior temperature evolves, the tidal response and tidal dissipation are updated in each time step.

2.7 Summary

The employed models for in each application (chapters P1–P11) are summarized in table 2.1.

chapter	body	tidal deformation	thermal evolution	rotational/orbital evolution
Běhounková et al., 2010; chapter P1	Enceladus, Earth-like exoplanets	1:1 or 3:2 SOR, free rotation; Maxwell rheology (using η_{eff}); time domain (FD-SH)	3D shell; BA; $\eta(T)$, Frank-Kamenetskii law; coupling, h_{tide}	not included; parametric study for orbital periods and spin-orbit resonances
Běhounková et al., 2011; chapter P2	Earth-like exoplanets	1:1 or 3:2 SOR; Maxwell rheology (η_{eff}); time domain (FD-SH)	3D shell; BA; $\eta(T)$ Frank-Kamenetskii law; coupling, h_{tide} and h_{rad} included	not included; parametric study for constant e and a
Běhounková et al., 2012; chapter P3	Enceladus	1:1 SOR; Maxwell rheology (η_{eff}); time domain, $\eta(T)$; localized ocean: mixed (free-surface/no-slip) boundary conditions	3D shell; BA; $\eta(T)$ Arrhenius law; coupling, h_{tide} and h_{melt} included, mixed (free-slip/no-slip, temperature/heat flux) boundary conditions	not included; parametric study for constant e; parametric study of e evolution for constant global tidal dissipation
Běhounková et al., 2013; chapter P4	Enceladus	1:1 SOR; Andrade-like rheology; time domain (FD-SH), localized ocean: mixed (free-surface/no-slip)	3D shell; BA; $\eta(T, d, \sigma)$ Arrhenius law, composite rheology; coupling, h_{tide} and h_{melt} included; mixed (free-slip/no-slip, temperature/heat flux) boundary conditions	not included; parametric study for constant e

Continued...

...Continued

chapter	body	tidal deformation	thermal evolution	rotational/orbital evolution
Běhounková et al., 2015; chapter P5	Enceladus	1:1 SOR; Andrade rheology; time domain (FD-SH), mixed (free-surface/no-slip) boundary conditions, parameterized η	not included	not included
Souček et al., 2016; chapter P6	Enceladus	1:1 SOR; elastic; faults included; uniform shell thickness; time domain (FE)	not included	not included
Walterová and Běhounková, 2017; chapter P7	terrestrial exoplanets	general potential eq. (2.2); Maxwell and Andrade rheology; time domain (FD-SH), parameterized η	not included	study of tidal torque and dissipation
Běhounková et al., 2017; chapter P8	Enceladus	1:1 SOR; elastic; faults included; variable shell thickness; time domain (FE)	not included	not included
Souček et al., 2019; chapter P9	Enceladus	1:1 SOR; Maxwel and Andrade-like; faults included; variable shell thickness; time domain (FE)	conduction, stationary (FE)	not included

Continued...

...Continued

chapter	body	tidal deformation	thermal evolution	rotational/orbital evolution
Walterová and Běhounková, 2020; chapter P10	terrestrial exoplanets	general potential eq. (2.2); Andrade rheology; NMT	1D parameterization; secular evolution of core's temperature; emerging magma ocean; impact of porosity	study of stable SOR; orbital-rotational-thermal coupling
Běhounková et al., 2021; chapter P11	Europa	1:1 SOR; Andrade-like; time domain (FD-SH)	3D shell; EBA; coupling, h_{tide}, h_{rad} (partitioning parameterization), h_{melt}; $\eta(T)$ Arrhenius law; coupled, h_{tide}; secular evolution of core's temperature	parametric study for different values of e, parametric evolution of e

Table 2.1: Summary of used methods for presented papers in chronological order.

2.8 List of symbols, definitions

General definitions	
δ_{ij}	Kronecker delta
$\mathcal{G}$	gravitational constant
$\mathbf{g}$	gravitational acceleration
Θ	Heaviside step function
Γ	gamma function
$\mathcal{P}_l$	Legendre polynomials, degree l
$\mathcal{P}_{lm}$	associated Legendre polynomials, degree l, order m
$\widehat{\bullet}$	image in the frequency domain
$\dot{\bullet}$	time derivative
$\bullet^{\mathrm{T}}$	transposition
$\mathrm{tr}(\bullet)$	trace
t	time
T	temperature
Deformed body	
r	radius
ϑ	co-latitude
φ	longitude
θ	sidereal time (rotation angle of the planet/moon)
$\dot{\theta} = \omega$	spin rate of the planet/moon
C	principal moment of inertia
R_{S}	radius of the surface
d	ice shell thickness/mantle thickness
T_{S}	temperature at the top of the shell
T_{B}	temperature at the bottom of the shell
ρ_0	reference density of ice shell/mantle
k	thermal conductivity
c_{p}	specific heat capacity
α	thermal expansivity
P	tidal period
Tidal potential	
$\mathcal{U}^{\mathrm{tide}}$	tidal potential
$\mathbf{f}^{\mathrm{tide}}$	tidal force
m_*	mass of the tide-raising body

r_*	distance from the center of the perturbed body to the tide raising body
S_*	angle from the axis from primary to secondary
e_* or e	eccentricity
a_* or a	semi-major axis
i_* or i	inclination
Ω_*	longitude of the ascending node
ω_*	argument of the pericenter
$F_{lmp}(i_*)$	inclination functions (Kaula, 1964)
$G_{lpq}(e_*)$	eccentricity functions (Kaula, 1964)
M_* or M	mean anomaly
$\dot{M} = n$	mean motion
ω_{lmpq}	frequencies of individual modes
	Tidal deformation
k_l	potential Love number, degree l
h_l	radial displacement Love number, degree l
l_l	horizontal displacement Love number, degree l
Q	tidal quality factor
Q^{-1}	tidal dissipation factor
ε	tidal phase lag
$(u_r, u_\vartheta, u_\varphi)$	components of displacement in spherical coordinates
$\mathbf{u}$	displacement vector
$\mathbf{e} = \frac{1}{2}\left(\nabla\mathbf{u} + \nabla^{\mathrm{T}}\mathbf{u}\right)$	incremental strain tensor
$\frac{1}{3}\mathrm{tr}(\mathbf{e})\mathbf{I}$	isotropic part of $\mathbf{e}$
$\mathbf{e}'$	deviatoric part of $\mathbf{e}$
$\mathbf{s}$	incremental (Cauchy) stress tensor
$\frac{1}{3}\mathrm{tr}(\mathbf{s})\mathbf{I} = -p\mathbf{I}$	isotropic part of $\mathbf{s}$
$\mathbf{s}'$	deviatoric part of $\mathbf{s}$
$\mathcal{T}$	secular torque, component orthogonal to the planetary equator
t_0	time of perigee passage
	Rheological parameters
$\overline{J}$	compliance operator
$J(t-t')$	compliance function/creep-response function
$\widehat{J}(\omega)$	complex compliance
$\widehat{\mu}(\omega)$	complex rigidity
λ	Lamé parameter
μ	Lamé parameter/shear modulus/rigidity
K	bulk modulus

η	viscosity
$\tau_{\mathrm{M}} = \eta/\mu$	Maxwell time
α_{A}	Andrade empirical coefficient
ζ_{A}	Andrade empirical coefficient
	Viscous flow
$\mathbf{v}$	velocity
$\boldsymbol{\sigma}$	stress tensor
π	dynamic pressure
$\boldsymbol{\sigma}'$	deviatoric part of $\boldsymbol{\sigma}$
h_{tide}	volumetric tidal heating
h_{rad}	volumetric radiogenic heating
h_{melt}	volumetric energy sink

Applications 3

This chapter describes the effects of tides on the Solar System bodies (Enceladus and Europa) and terrestrial exoplanets bodies. First, we concentrate on general features of coupled thermal-tidal model and susceptibility of icy moons and terrestrial planets to tidal dissipation (section 3.1). Then we discuss the applications for Europa (section 3.2), including possible observable manifestations of the activity triggered by tidal dissipation. For Enceladus (section 3.3), we describe the impact of tidal dissipation on thermal evolution and the presence of thermal convection. We also focus on the impact of the faults on tidal deformation using the tailored model. The impact of tidal dissipation on the habitability of exoplanets around low mass stars is in section 3.4. This section is also dedicated to the discussion of the tidal torque and the first-order tidal effect on the coupled rotational-orbital-thermal evolution of a planet without a companion. The particular details of the models and the employed method depend on fast-evolving knowledge about the moons and planets and on the development of the methods presented in chapter 2.

3.1 Susceptibility to tidal dissipation

General features and principles of the thermal evolution susceptibility on the tidal dissipation have been described in Běhounková et al. (2010). The coupled thermal-tidal model, where tidal dissipation is repeatedly updated with changing 3D temperature field, and the orbital-rotational parameters are constant, was also applied to the icy shell of an Enceladus (section 3.3) and silicate mantle of Europa (section 3.2) and exoEarths (section 3.4).

The relationship between the thermal evolution and tidal heating can be illustrated by the dependence of the local tidal dissipation rate on the temperature and viscosity (fig. 3.1). In general, the dissipation rate on the tidal frequencies is increasing with increasing temperature and hence decreasing viscosity (moving from A to B in fig. 3.1). This is a key characteristic that leads to positive feedback between the temperature and tidal dissipation rate. Two basic evolutionary scenarios are predicted, starting from a convective (statistic) steady-state without tidal heating and then including tidal dissipation. In the first case, a new statistical steady

state with an increased internal temperature is found. An exponential temperature increase is observed in the second scenario, leading to thermal runaways unless a regulating mechanism is triggered. The transition between the scenarios is complex, can be abrupt, and results from a complex interplay between the efficiency of heat transfer and heat sources. Roughly, if the global tidal dissipation is lower than the global power transferred through the surface if no tidal dissipation is included, then the former scenario is observed. The second scenario is expected if the global tidal dissipation is comparable to or higher than heat loss through the surface.

The existence of the maximum volumetric dissipation rate (fig. 3.1, point M), i.e., the point breaking the positive feedback between the temperature and dissipation, is one mechanism allowing us to reach a new equilibrium with an increased temperature in the second scenario. Crossing this point is possible for icy materials. For example, the maximum tidal dissipation rate is reached for the viscosity $\sim 6 \cdot 10^{13}$Pa s for Enceladus (Běhounková et al., 2012), which is a value within an expected viscosity range for ice (e.g., Goldsby and Kohlstedt, 2001) albeit on the lower edge of the expected range. However, reaching the breaking point is not plausible for silicates before reaching the melting temperature. Reaching the melting temperature is another possible and natural mechanism stopping the runaway and/or change the equilibrium. An end-member scenario, where any produced melt is instantly extracted, resulting in volcanic activity for silicate mantles (Běhounková et al., 2021) or melting of the ice shell (Běhounková et al., 2012), naturally limits the temperature and stops the runaway. If melt stays embedded in the solid matrix, latent heating inhibits and delays the temperature increase. The material begins to melt gradually, building a system of interconnected channels. Once the local melt fraction reaches the disaggregation point, the rigidity is strongly affected and sharply decreases. As a consequence, the tidal dissipation drops and the response to the tidal loading changes (Walterová and Běhounková, 2020). Combined with strongly decrease viscosity and more effective heat transport, a new equilibrium near the disaggregation point can be reached.

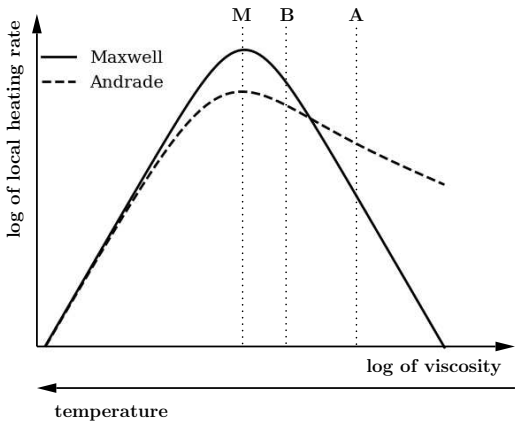

Figure 3.1: Illustration of the local dissipation rate for a given tidal strain rate, loading period, and shear modulus as a function of viscosity for the Maxwell model (solid line) and the Andrade model ($\alpha_A = 0.3$, $\zeta_A = 1$ dashed line).

Due to the long-wavelength (degree $l = 2$) tidal loading, the tidal heating has a 3D character and leads to a tidal dissipation pattern having the corresponding long-wavelength component. The maximum local heating rate is observed in the polar areas (provided liquid layer lies beneath the shell), the minima are located in the equatorial area in the vicinity of the tidal axis for 1:1 and 3:2 spin-orbit resonances. On shorter-wavelength, the dissipation is modulated by the temperature pattern originating in the convection, and it is usually increased in the hot upwellings and decreased in the cold downwellings. In return, the tidal dissipation can break the relatively uniform distribution of convective planforms, can help focus the hot upwellings in the areas with the highest dissipation and create sheet-like hot structures near the bottom boundary. Additionally, the subadiabatic temperature gradient is reached (the temperature is slightly higher under the stagnant lid than above the lower boundary layer) consistent with convection with significant internal heating characteristics (e.g., Parmentier et al., 1994) and favoring the melting at the base of the stagnant lid (Běhounková et al., 2012, 2021).

3.2 Europa

Europa's surface is young (Bierhaus et al., 2009). The ice shell is tectonically modified (Figueredo and Greeley, 2004; Kattenhorn and Prockter, 2014) and conceals a salty ocean (Kivelson et al., 2000) beneath. Europa's deep interior is likely differentiated into an iron-rich core and a silicate mantle (Anderson et al., 1998; Gomez Casajus et al., 2021). The silicate mantle is therefore in direct contact with the salty ocean. This setting provides an environment hospitable to life beyond the Earth. The habitability is, however, conditioned by the chemical interaction with the rocky seafloor (Vance et al., 2016) and by the heat released from the deep interior to the seafloor and magmatic activity (Altair et al., 2018). The heat output from the silicate mantle is controlled by the available heat sources and by heat transfer from the silicate mantle and iron-rich core to the ocean. Global radiogenic heating, a major energy source, has been imprinted during the accretion, and it decays with time (Hussmann et al., 2010). In contrast, Europa's global tidal dissipation can strongly fluctuate with time due to the locking into 1:1 spin-orbit resonance and due to the interaction with Io and Ganymede through the Laplace resonance (Hussmann and Spohn, 2004).

Using the model coupling the tidal heating and thermal evolution with instantaneous melt extraction (chapter 2), we investigate Europa's thermal state and heat released from the silicate mantle, depending on the heat extraction and available heat sources. We try to identify the requirements for melting sustainability until

the present day (Běhounková et al., 2021). Moreover, we indicate possible measurements by future missions (JUICE and Europa Clipper), hinting at recent volcanic activity and providing constraints on the available heating.

We consider thermal convection controlled by the temperature-dependent viscosity with parameters consistent with experimental constraints on dry olivine (e.g., Karato, 2012). Similar to thermal convection, the tidal dissipation is also controlled by the temperature-dependent effective viscosity using Andrade-like rheology. Besides the rheological parameters, the tidal dissipation depends on the orbital eccentricity. The eccentricity evolution is unknown, and we treat it as a parameter. The eccentricity is considered either constant in time or parameterized with periodic variations as expected due to Laplace resonance (Hussmann and Spohn, 2004), considering the eccentricity varying by factor 2. Due to lack of direct information on the concentration of radiogenic element content, we test low- and high-content based on chondrite end-members composition (Hussmann et al., 2010).

The results suggest that the heat transfer through the cold upper boundary layer dominates the heat flux from the mantle to the ocean, but heat loss by melt production contributes significantly during the early stages of evolution. A pulse in the melting production occurs during the onset of convection. Radiogenic heating is a dominant heat source. It, however, decays relatively fast with time. For the current value of eccentricity, tidal dissipation corresponds only to approximately 10 percent of the heat sources initially, but it increases to 40 percent at the present day. The temporal convection and melting patterns reconfiguration well demonstrate the increasing importance of tidal dissipation with time: Once the convection is well established and radiogenic heating dominates, the melting is more-or-less homogeneously distributed and is only modulated by cold downwellings. At the later stages of evolution, tidal dissipation keeps the mantle warmer in the polar regions, where the tidal dissipation is largest, and melting occurs preferentially at high latitudes.

If periodic eccentricity variations are considered, the tidal dissipation can exceed the radiogenic power during periods of enhanced eccentricity in the last two billion years. The radiogenic power still controls the melting rate at the early stages of evolution. However, the melting rate is strongly modulated by eccentricity changes during the later stages. Due to the limited efficiency of the heat transfer, the results also suggest that the melt production still occurs during periods of enhanced eccentricity, even for models with low radiogenic heating during the last billion years. Remarkably, the present melting rate can depend on the way the eccentricity is currently evolving. If the eccentricity is presently increasing, Europa should be at a minimum of the melt production. On the other hand, if the eccentricity is currently decreasing, a significant heating rate and melt production are predicted in the recent

past.

Analyzing gravity measurements performed by the Europa Clipper mission may reveal long-wavelength variations in the gravity field (Verma and Margot, 2018) and may point to mass anomalies at the pole as predicted by the results. Geological mapping of Europa's surface (Figueredo and Greeley, 2004; Leonard et al., 2018) also suggested that ice shell thickened in the recent past. Therefore, our models would be consistent with an eccentricity and heating decrease, possibly hinting at ongoing active melt production. Precise determination of Galilean moons' ephemerides obtained by the JUICE and Europa Clipper missions (Dirkx et al., 2017) can provide information about Europa's orbital dynamics. Determination of the mean motion rate for moons in Laplace resonance could constrain the present-day dissipation rate (Lainey et al., 2009).

Silicate melts exposed at the seafloor during magmatic pulses could also induce volatile release from magma degassing, destabilizing a volatile-rich crustal layer or associated hydrothermal activity. The detection of these volatile species would confirm the predicted large-scale seafloor activity. At present, due to declining activity, we estimate that the volcanic release of CO_2 at the seafloor would hardly exceed the rate provided by surface radiolytic processes, and the CO_2 signature would be difficult to distinguish from the background CO_2. The detection of CH_4 might be more discriminating as it would hint at mantle composition. The estimated production of H_2 can be slightly lower than production by sputtering processes (Cassidy et al., 2013).

3.3 Enceladus

Despite its small size, Enceladus is one of the most active bodies in the Solar System. It has a tectonically modified ice shell, and Enceladus' surface geology reflects its complex history (Nahm and Kattenhorn, 2015). Its activity is highly symmetrical along the current tidal axis (Crow-Willard and Pappalardo, 2015). It, however, mainly concentrates in the very young south polar region (SPR). Furthermore, the exceptional eruption of water vapor is connected to the highly active SPR and it originates in four warm tectonic ridges (e.g., Porco et al., 2006; Hansen et al., 2006; Spencer et al., 2006) informally known as "tiger stripes". The geysering activity also provides a unique opportunity to sample its interior.

A challenging question for Enceladus is, however, maintaining the internal liquid ocean. Due to only limited radiogenic heating, tidal dissipation in an icy shell above at least a local water reservoir (Tobie et al., 2008) was suggested to feed the observed activity and heat loss through SPR (Howett et al., 2011). Similar to other close-in

moons of giant planets, Enceladus is captured into 1:1 spin-orbit resonance. The eccentricity evolution is driven by mean motion resonance with Dione, and Saturn's quality factor controls the equilibrium tidal heating (Meyer and Wisdom, 2007). For a conventional dissipation in Saturn, the equilibrium tidal dissipation can be up to one order of magnitude smaller than the observed heat loss. This discrepancy can be explained by periodic (Shoji et al., 2013) or episodic heat loss (O'Neill and Nimmo, 2010). Alternatively, the quality factor of Saturn has to be small (Lainey et al., 2012), which could mean that the inner satellites are young (Ćuk et al., 2016) unless, e.g., resonance locking scenario requiring frequency-dependent quality factor takes place (Fuller et al., 2016).

Susceptibility to tidal dissipation

The presence of convection in the icy satellites can induce an enhanced activity, which manifests as increased heat flux or through geological consequences. Convective processes possibly fueled by tidal dissipation had been also speculated to play a role in tectonic activity at Enceladus' south pole (Nimmo and Pappalardo, 2006; Barr, 2008; Mitri and Showman, 2008; Roberts and Nimmo, 2008; Stegman et al., 2009; Han et al., 2012). To investigate the convection-induced activity and to constrain the evolution of the liquid reservoir, we applied the method described in chapter 2 coupling tidal heating, thermal evolution, and including an instantaneous melt extraction model. We considered Enceladus with thick ice shell and local or global water reservoir/ocean at the base of the ice shell.[1] Temperature dependence of viscosity complies with laboratory measurements (Durham et al., 2001; Goldsby and Kohlstedt, 2001). We tested different temperature dependencies for the transient creep through effective viscosity for the Maxwell rheology (e.g., Budd and Jacka, 1989). Although the orbital eccentricity can vary, it is kept constant, and various values are tested. The typical runaways time scales are compared to eccentricity damping scales using the relationship by Meyer and Wisdom (2008) to infer plausibility of the periodic behavior. Starting from a state with negligible tidal dissipation rate and increasing eccentricity, the temperature increases towards the melting temperature, and dissipation rate increases for a model with maximum tidal heating reached for a temperature around or higher than the melting temperature (cf. fig. 3.1). The evolution is more complex for models with maximum tidal heating for a temperature lower than the melting temperature. The global tidal dissipation can decrease once and if the temperature corresponding to the maximum heating is

[1] Note that Thomas et al. (2016) later changed the view on Enceladus' structure substantially by measuring a large amplitude of physical libration, confirming the presence of the global ocean and leading to a substantial thinner ice shell.

exceeded. This decrease can be later partly compensated by a temperature growth in cold parts, including the stagnant lid, due to the increased heating. Independent of assumed rheological models, the temperature reaches the melting point if eccentricity exceeds the critical value. For at least a hemispheric ocean, the eccentricity larger than three times the currently observed values induces the melting. The melting can be so intense that it overcomes the crystallization rate at the base of the ice shell. In these cases, the stress induced by the volumetric changes due to the melting can trigger the brittle failure of the material and can explain the tectonic activity. However, the melting events should be brief as they are associated with increased heat flow (and cooling) and rapid eccentricity damping depending on Saturn's quality factor (Meyer and Wisdom, 2008).

The tidal dissipation can also help trigger the onset of convection in the icy satellites in unfavorable settings (Běhounková et al., 2013). The numerical simulations can allow us to understand the conditions for the convection initiation better and to constrain the duration and periodicity of enhanced activity as described above (cf. Běhounková et al., 2012). The conditions for onset of convection in systems heated from below and/or from within has been extensively studied (e.g., Davaille and Jaupart, 1994; Barr and Pappalardo, 2005; Solomatov and Barr, 2006). Barr and McKinnon (2007) established from scaling laws the conditions for the onset of convection in Enceladus, taking into account the interplay of various creep mechanisms. We followed the study using the numerical experiments of coupled thermal-tidal evolution. Again, we considered a thick ice shell and a global or localized ocean beneath the shell. The eccentricity is again kept constant to understand the impact of heterogeneous tidal dissipation on the onset of convection, and a parametric study for different eccentricities regulating the available sources of internal heating was performed. We use the rheological properties sensitive to temperature, grain size, and convective stress to describe the viscosity characterizing the viscous flow. The considered deformation mechanisms include dislocation creep, grain size sensitive creep, and diffusion creep (Goldsby and Kohlstedt, 2001). The Andrade-like rheology is described to comply with the body's response on the tidal time scale. The coupled numerical simulation showed that the onset of convection, i.e., radial heat transport dominated by convection, is controlled by the grain size and the tidal heating rate as the diffusion creep is the prevailing deformation mechanism and it strongly depends on the grain size but is independent of the stress. The onset of convection is observed for grain size smaller than or equal to 0.5 mm. The presence of heterogeneous internal heating increases the temperature anomalies, locally reducing the viscosity, increasing the buoyancy, and favoring the onset of convection. If significant tidal dissipation is included, the critical grain size needed for triggering the convection

shifts to $1 - 1.5$ mm. However, for these values, the temperature reaches the melting temperature, and melt production is triggered. Grain size smaller than 1.5 mm, can be reached by limiting the grain growth by pinning if few percent of impurities present and by dynamic recrystallization during increased stress periods possibly associated with tidally induced melting events.

Tidal deformation and activity prediction

Besides the thermal evolution coupled with tidal heating, we also concentrated on the tidal deformation of the ice shell. We further investigated the stress distribution and possible impact of the shell's properties on the timing of the observed geysering activity. In later studies, we have also included the effect of variable ice shell thickness and the presence of faults.

Enceladus' interior structure is mainly inferred from the shape (Thomas et al., 2007) and long-wavelength gravity measurements (Iess et al., 2014). Gravity variations are, however, smaller than expected from the surface topography suggesting a compensation mechanism. An obvious choice of compensation is the existence of at least a local subsurface water reservoir and locally reduced ice thickness (Collins and Goodman, 2007; Iess et al., 2014; McKinnon, 2015). The existence of a water reservoir is also consistent with the detection of salts in material ejected by geysers (Postberg et al., 2009, 2011). Detection of silicon-rich particles (Hsu et al., 2015) and H_2 (Waite et al., 2017) even indicate hydrothermal reaction between water and silicates.

Furthermore, the geysering activity is not constant in time, but it is modulated by diurnal tides (Hedman et al., 2013; Nimmo et al., 2014; Ingersoll and Ewald, 2017; Ingersoll et al., 2020) on 1.37 day period. However, the observed activity is several hours delayed compared to prediction based on simple tidal models (Hurford et al., 2007; Nimmo et al., 2014). The observed time lag is usually attributed to the eruption mechanism, processes on the faults, or a delay in stress variation associated with the viscoelastic structure of the moon. The last possibility is tested in Běhounková et al. (2015) taking into account the Andrade rheology (see chapter 2). We considered a parameterized temperature structure for which we investigated the impact of ice shell thickness, the extent of axisymmetric viscous anomaly centered at the south pole, and the extent of the ocean. We furthermore assumed a thin lithosphere explaining the observed high local heat fluxes. Inspired by Hurford et al. (2007), we assumed that the eruption rate is proportional to the normal stress applied to the tiger stripes. We found that the two classes of models with a low viscosity convective region can explain the lag. The first class of successful models contains a regional polar sea extending $\sim 50^\circ$ from the south pole and only weakly

depending on the ice shell thickness. In these cases, the tidal heat production ($< 0.5\,\mathrm{GW}$) cannot compensate for the estimated heat loss $1 - 2\,\mathrm{GW}$ corresponding to this model temperature structure. The second class requires a thick ice shell and allows for the global ocean. The estimated heat production ($\lesssim 10\,\mathrm{GW}$) can compensate for the estimated heat loss in favorable cases considering low viscosity. Nevertheless, the compensation of the heat loss by tidal dissipation in the ice shell is very difficult in general.

The later measurement of the amplitude of physical libration stirred the knowledge about Enceladus' structure (Thomas et al., 2016). The large observed amplitude provides strong evidence for the existence of the global ocean and strongly limits the ice shell thickness. The joint topography-gravity-libration inversions (Čadek et al., 2016; Beuthe et al., 2016; van Hoolst et al., 2016; Hemingway et al., 2018; Čadek et al., 2019) estimated the average ice shell thickness to be around 20 km and they predict substantial ice shell thickness variations with minimum thickness only a few kilometers beneath SPR. Thin ice shell combined with rapid transport of hydrothermally derived products from the ocean floor strongly suggests that the tiger stripes are passing through the whole ice shell and can strongly affect Enceladus' shell's propensity to deform. In a series of papers (Souček et al., 2016; Běhounková et al., 2017; Souček et al., 2019), we studied the impact of the variable ice shell thickness and presence of faults passing through the whole thickness of the shell on local and global deformation, heat production, and on the predicted variation in geysering activity. We represent the tiger stripes as fault zones with negligible frictional and bulk resistance, i.e., rigidity and bulk moduli drops several orders of magnitudes in the fault zone. Such a representation, therefore, maximizes the impact of the tiger stripes on the tidal deformation. The surface geometry corresponds to the observed geometry (Porco et al., 2014) passing vertically through the shell. Considering the elastic rheology, variable ice shell thickness and no faults, the stress amplitude is strongly influenced by the local ice shell thickness, increasing the stress locally by a factor ~ 6 compared to a model with uniform thickness (for models having the same average ice shell thickness). For a model with faults and no thickness variations, the stress field is locally affected in the vicinity of fault zones, especially in faults' tips as theoretically expected. Short-wavelength stress anomalies are also created in between the faults. A similar stress pattern, albeit with increased amplitude, is predicted if both thickness and faults are included. Additionally, the stress regime (from compression to extension and vice versa) can change with depth, indicating an important role of bending stresses in SPR. The local displacement is less affected by the local changes. Interestingly, only if both variable ice shell thickness and faults are considered, the displacement field is significantly influenced, and it is locally

increased up to a factor of seven.

Globally, the deformation is best represented by the Love number. For the model with a 20km thick ice shell with uniform thickness and no faults, the deformation is characterized by $k_2 = 0.014$. Due to the aspherical character of faults and variable ice shell thickness, the spectral splitting is predicted with a more significant increase at order 2. The Love number can increase to $k_{20} = 0.026$ and $k_{22} = 0.035$ if faults and variable ice shell thickness are included. Furthermore, spectral interaction leaks beyond degree 2. The spectral power of the induced gravitational potential at the surface at degree 3 is approximately 6% of power at degree 2.

Also, for models with faults, we can again predict the observed geysering activity. In this case, we assume that the eruption rate is proportional to the applied average normal displacement jump across the fault zone (i.e., to opening and closing of the faults). We predict a possible temporal heterogeneity of activity for models with faults, i.e., the maxima of activity are shifted by several hours for individual faults. On average, we again observe approximately five hours delay between the predicted and observed activity. The predicted delay is even higher for models with variable ice shell thickness and cannot be explained even if the largest possible delay due to viscoelastic behavior is included, hinting at an alternative explanation of the lag (e.g., Kite and Rubin, 2016).

The increased stress and deformation rate connected to the thin ice shell with variable thickness and presence of faults can lead to increased tidal dissipation, especially in SPR. For a model with Andrade-like rheology, we also estimated heat production (Souček et al., 2019). Due to the thin ice shell, the convection is not probable (Běhounková et al., 2013) even for low viscosities. Again, even for the most favorable viscosity value at the melting point, the global heat production in the ice shell is significantly lower ($\sim 2\,\mathrm{GW}$) than the predicted conductive heat loss for a thin shell ($40\,\mathrm{GW}$). Moreover, this predicted heat loss is approximately three times higher than the equilibrium tidal power (Meyer and Wisdom, 2007) for the revised value of Saturn's quality factor (Lainey et al., 2012), but it may be consistent with resonance locking scenario (Fuller et al., 2016). To conclude, our results suggest that the tidal dissipation in the ice shell cannot compensate for the heat loss. If the current state is close to an energy equilibrium, tidal energy dissipated in deeper parts seems more plausible. Dissipation due to both ocean tides (Matsuyama et al., 2018) and radiogenic heating are, however, likely low. The libration triggered turbulent dissipation in the ocean (Wilson and Kerswell, 2018) or tidal dissipation in porous water-fill core (Choblet et al., 2017) can explain significant heat loss. The tidally heated core is an especially tempting possibility as it can also explain the observed hydrothermal activity (Hsu et al., 2015; Waite et al., 2017). Nevertheless,

this is still under debate (Kang et al., 2020).

3.4 Terrestrial exoplanets

Habitability of exoEarths

The habitability of worlds beyond the Solar System and understanding the uniqueness of the Earth often drive exoplanetary research. The indirect and the most successful detection techniques of exoplanets tend to favor the discovery of short-period planets around low mass stars (see, e.g., Wright and Scott, 2013, for a summary). Remarkably, the distance of the traditional habitable zone (HZ) to the host star strongly decreases with decreasing star mass due to strong reduction of star's luminosity and requirement of the liquid water on the surface (Kasting et al., 1993). The Earth-like planets within the HZ are, therefore, prone to be influenced by tides, and they are predicted to be fast tidally locked for a low mass star $m_* \lesssim 0.5 m_{\rm Sun}$ (Lammer et al., 2010). The tidal locking affects the stability of the climate (e.g., Kite et al., 2011). The tidally induced runaways as described above can result in large-scale melting, can also induce intense magmatism as observed on Io (e.g., Lopes and Williams, 2005) and a rapid magmatic resurfacing, and therefore represents yet another obstacle in planet's habitability (Běhounková et al., 2011). For constant orbital and rotational parameters and temperature-dependent viscosity, we have shown that the reciprocal value of the runaway time scale depends linearly on the global dissipated power when the tidal dissipation is activated. For exoEarth in the HZ of $0.1 m_{\rm Sun}$ star and locked in 1:1 spin-orbit resonance, the thermal runaways are predicted for a sufficiently high eccentricity ($e > 0.02$ at 4 days orbital period, $e > 0.2$ for 10 days orbital period for efficient heat transfer, i.e., for a low viscosity dependence on temperature). For planets in 3:2 spin-orbit resonance, the runaways are estimated for orbital periods lower than 12 days, and it is only weakly dependent on the eccentricity. We also found that the thermal runaways can limit the HZ for host star mass $m_* \lesssim 0.4 m_{\rm Sun}$.

Torque and rotational-orbital evolution

The previous sections concentrated on bodies locked in spin-orbital resonances and on the susceptibility of their thermal evolution to tidal heating. In this section, we first deal with the computation of tidal torque and tidal dissipation for differentiated terrestrial exoplanets with general spin-orbit ratio (SOR), i.e., including planets outside the spin-orbit resonances using approaches in both time-domain (Walterová and Běhounková, 2017) and frequency domain (Walterová and Běhounková, 2020) and

taking into account the Maxwell and the Andrade rheology. Then we discuss long-term evolution for chosen exoplanets with zero obliquity incorporating parameterized thermal evolution, possible formation of a melted layer, and including consistently evolving spin rate and orbital parameters.

The long-term stability of the spin rate requires zero time average of tidal torque. The graph describing secular tidal torque as a function of spin-orbit ratio is complex and depends on the forcing frequencies and rheological properties. The contribution of individual modes (frequencies) is described by the Kaula-Darwin expansion (eq. (2.34b)). For a low viscosity regime, only one stable spin is possible, which corresponds to pseudo-synchronization as predicted by constant time lag rheological description (e.g., Mignard, 1979). With increasing viscosity (and keeping other parameters constant), the number of stable SOR associated with spin-orbit resonances increases for both the Maxwell and the Andrade rheology. The torque as a function of SOR has "kink-shaped" character around the stable spin states. The height of these peaks around the equilibrium SOR determines its stability and depends on the rheology and rheological parameters.

For planets captured into the stable spin-orbit resonance from above (i.e., planets are rotating fast after their accretion), similarly as expected in the Solar System, it is insightful to investigate their highest possible stable spin state they are passing during the despinning. Considering non-zero constant eccentricity, the boundaries between the stable spin-states have a complex character for both Andrade and Maxwell rheologies. For high mantle rigidity (rheology dominated regime), the stable spin is controlled by the viscosity. It depends on both viscosity and rigidity for the low rigidity (self-gravity-dominated deformation regime).

Two regimes roughly characterize the dependence on eccentricity with different types of stable spin states. The first regime is observed for rheological properties leading to the Maxwell time being shorter than the leading loading period (i.e., low viscosity regime). It is characterized by pseudo-synchronous rotation with SOR approximately given by $1 + 6e^2$ (e.g Dobrovolskis, 2007). In the second regime, the first stable spin-orbit resonance again depends on the viscosity, and it is also controlled by the eccentricity: the higher the eccentricity, the higher the stable SOR. Remarkably, the spin-orbit resonance depends also on the planet radius and the core mass fraction (CMF). Planets with small radii or low CMFs tend to be captured into higher spin-orbit resonances.

Tidal heating is strongly influenced by rheology, and consequently, the choice of rheology can have a large impact on the internal thermal evolution, as already discussed (section 2.2). Investigating tidal dissipation as a function of SOR, the magnitude of global tidal heating in the Andrade models increases with SOR and

attains minimum for synchronous rotation, whereas the heating for high SOR and the Maxwell model is almost constant. We also observe local minima in global heating for low spin-orbit resonances for the Maxwell model. The depth of local minima is controlled by both eccentricity and viscosity. For the Andrade rheology, the local minima can also be reached for low spin-orbit resonances. They are, however, very shallow.

Investigating global tidal dissipation for the highest stable spin state and considering the Andrade rheology, we can conclude that the mantle rigidity and viscosity have a significantly larger impact on the global tidal dissipation than different spin-states and orbital eccentricities. Only transition from 3:2 to 1:1 SOR and low eccentricity can result in a significant drop in the tidal dissipation. For 1:1 SOR, the tidal dissipation depends on eccentricity as approximately e^2, and it is almost independent of eccentricity for higher resonances as also expected theoretically (e.g., Běhounková et al., 2011). For terrestrial exoplanets, we can also conclude that the global tidal dissipation increases with planetary radius or decreasing core mass fraction as a simple consequence of differing mantle volume.

In Walterová and Běhounková (2020), we have also investigated the coupled evolution employing a semi-analytical model, parameterized 1D heat transfer including effects of the emerging magma ocean and self-consistently calculated tidal dissipation, spin state, eccentricity, and semi-major axis. At the beginning of the evolution, the planet despins fast into the first stable spin-orbit resonance, which value depends on the reference viscosity. Due to the orbital and rotational parameters, the planet is strongly tidally loaded and consequently strongly tidally heated. The presence of a significant source of internal energy inevitably results in a decrease in viscosity and rigidity due to the temperature increase and the presence of melt. The presence of melt eventually leading to tidal heating drop once the disaggregation point is reached. A new temporary thermal equilibrium is observed. Evolving eccentricity eventually leads to spin-orbit resonance destabilization and transition into lower spin-orbit resonance. This resonance is accompanied by a drop in the tidal dissipation rate. Again, a new equilibrium is reached, and the cycle repeats until the synchronous resonance is attained. Final despinning into 1:1 SOR eventually slows down the orbital evolution and can help maintain long-term stable orbital eccentricity.

Conclusions 4

The papers summarized in this thesis describe possible manifestations of tides on icy satellites of giant planets and terrestrial planets beyond the Solar System using numerical simulations. The numerical methods range from the classical but fast method to assess the first-order impact of tides to newly developed tools tailored to individual bodies using the finite element method. Special attention was paid to the coupling of the models to describe feedback between thermal evolution and tidal heating.

The presented applications contributed to a better understanding of the susceptibility of thermal evolution to tidal dissipation and to the investigation of general aspects of thermal-rotational-orbital evolution. The modeling effort introduced here can also be used to interpret the results of past and future missions. In particular, the presented models may help explain data collected by past missions Galileo and Cassini. In the future, Jupiter's system is a primary target of ESA's mission JUICE (Grasset et al., 2013) scheduled to launch in 2022 and NASA's Europa Clipper mission planned to be launch in 2024 (Howell and Pappalardo, 2020). Also, several mission concepts focusing on Enceladus are currently under study (Neveu et al., 2020; Howell et al., 2020; Ermakov et al., 2020; Vance et al., 2021; Marusiak et al., 2021) and obtained results can be used to assess the required accuracy of measurements.

In particular, we investigated here the conditions for the presence of melt in Europa's silicate mantle. Even though silicate volcanism is significantly reduced compared to Io, we predict that the silicate melt can be produced during almost the entire history and may influence the ocean chemistry. Observations by future missions may confirm the ongoing seafloor magmatic activity and their focusing at high latitudes as predicted by our model.

For Enceladus, we examined the possibility of explaining the observed heat loss by tidal dissipation, especially by the dissipation in the ice shell. We investigated the extent and stability of the internal ocean, concluding that a deeper heat source might be essential for sustaining the ocean. Furthermore, the presented results suggest that four prominent faults combined with the variable ice shell thickness can locally increase the tidal deformation by almost an order of magnitude and can strongly change the stress regime due to the bending stresses. The timing of the

observed geysering activity modulated on tidal period combined with the recently observed changes on longer periods (Ingersoll and Ewald, 2017; Ingersoll et al., 2020) remains puzzling.

Beyond the Solar System, the increasing number of detected exoplanets provides a unique statistical set that may improve our knowledge about planetary evolution despite the limited data we so far have about terrestrial exoplanets. Describing the relationship between the internal dynamics and measurable quantities could constrain the conditions on extrasolar worlds. Here, we identified the conditions for the thermal runaways possibly affecting their habitability and triggering large-scale magmatic activity. We also showed that the tidal dissipation is highly increased by locking into high spin-orbit resonance for low eccentricities. For the semi-analytical thermal-orbital-rotational evolution model, we demonstrated that the evolution of strongly tidally loaded exoplanets could continue as a sequence of thermal equilibria determined by the spin-orbit resonance. Once in synchronous rotation, the tidal evolution slows down, and orbital eccentricity can be maintained for long periods.

Future work will follow two closely linked directions: method development and broadening of the applications. A challenging aspect of satellite and planetary evolution remains the coupling of the thermal and orbital evolutions. Many ingredients are yet to be included in the model. The effect of an outer perturber and non-zero obliquity will be investigated. Planets with non-zero obliquity can result in a different spin-orbit resonance, and the obliquity tidal heating can add to the thermal budget. Moreover, stable non-zero obliquity corresponding to the Cassini state may prevent cooling once the eccentricity decreases. In the future, the coupled thermal-tidal evolution will also be applied to the Earth-Moon system, and the coupled orbital-thermal evolution of Jupiter's system is planned in cooperation with colleagues from the University of Nantes.

For future applications, it is also important to include a more realistic description of the heat transfer. Due to the exponential runaways, especially for the silicate mantles, a large amount of melting is expected. We have so far used only a very simple treatment of melt transport. A more complex model inspired by Io (Moore, 2003; Bierson and Nimmo, 2016; Moore et al., 2017; Spencer et al., 2020, 2021) is planned to be included. The improved model could help better understand the evolution of exoplanets and assess the limits of the approaches used so far. Evolutionary models of Europa can also benefit from the more detailed description.

For modeling deformation and stress, it is also essential to assess the possible contribution of the stress on several time scales. Besides eccentricity-driven diurnal tides with physical libration, we plan to include loading due to obliquity-driven tides for Europa, non-synchronous rotation, the changes in the shell orientation,

and the recession of the orbit. We will continue to model the viscous flow in the shell of uneven thickness and the effect of the possibly overpressurized ocean due to global crystallization on the longest time scale. Similar to other approaches, we assume that the stresses on individual periods are independent. This simplification, however, may not hold, especially if non-linear rheology is included. We are planning to study a possible interaction of deformation on different periods. For example, friction along Enceladus' tiger stripes leads to the permanent deformation and non-zero background stress constant on tidal period (Pleiner Sládková et al., sub). The background stress would tend to relax on longer periods, and it would inevitability trigger the long-term viscous flow.

Bibliography

A, G., J. Wahr, and S. J. Zhong (2014). "The effects of laterally varying icy shell structure on the tidal response of Ganymede and Europa". In: *J. Geophys. Res. Planets* 119, pp. 659–678. DOI: 10.1002/2013JE004570.

Akinsanmi, B. et al. (2019). "Detectability of shape deformation in short-period exoplanets". In: *Astronomy & Astrophysics* 621, A117. DOI: 10.1051/0004-6361/201834215.

Alnaes, M. S. et al. (2015). "The FEniCS Project Version 1.5". In: *Archive of Numerical Software* 3.100, pp. 9–23. DOI: 10.11588/ans.2015.100.20553.

Altair, T., M. G. de Avellar, F. Rodrigues, and D. Galante (2018). "Microbial habitability of Europa sustained by radioactive sources". In: *Sci. Rep.* 8.1, 260. DOI: 10.1038/s41598-017-18470-z.

Anderson, J. D. et al. (1998). "Europa's differentiated internal structure: Inferences from four Galileo encounters". In: *Science* 281.5385, pp. 2019–2022. DOI: 10.1126/science.281.5385.2019.

Barnes, R., B. Jackson, R. Greenberg, and S. N. Raymond (2009). "Tidal Limits to Planetary Habitability". In: *Astrophys. J. Let.* 700.1, L30. DOI: 10.1088/0004-637X/700/1/L30.

Barnes, R., S. N. Raymond, B. Jackson, and R. Greenberg (2008). "Tides and the Evolution of Planetary Habitability". In: *Astrobiology* 8.3, pp. 557–568. DOI: 10.1089/ast.2007.0204.

Barr, A. C., V. Dobos, and L. L. Kiss (2018). "Interior structures and tidal heating in the TRAPPIST-1 planets". In: *Astronomy & Astrophysics* 613, A37. DOI: 10.1051/0004-6361/201731992.

Barr, A. (2008). "Mobile lid convection beneath Enceladus' south polar terrain". In: *J. Geophys. Res.* 113, E07009. DOI: 10.1029/2008JE003114.

Barr, A. and W. McKinnon (2007). "Convection in Enceladus' ice shell: Conditions for initiation". In: *Geophys. Res. Let.* 34, L09202. DOI: 10.1029/2006GL028799.

Barr, A. and R. Pappalardo (2005). "Onset of convection in the icy Galilean satellites: Influence of rheology". In: *J. Geophys. Res.* 110, E12005. DOI: 10.1029/2004JE002371.

Baumeister, P. et al. (2020). "Machine-learning Inference of the Interior Structure of Low-mass Exoplanets". In: *Astrophys. J.* 889.1, 42. DOI: 10.3847/1538-4357/ab5d32.

Běhounková, M., O. Souček, J. Hron, and O. Čadek (2017). "Plume Activity and Tidal Deformation on Enceladus Influenced by Faults and Variable Ice Shell Thickness". In: *Astrobiology* 17, pp. 941–954. DOI: 10.1089/ast.2016.1629.

Běhounková, M., G. Tobie, G. Choblet, and O. Čadek (2013). "Impact of tidal heating on the onset of convection in Enceladus's ice shell". In: *Icarus* 226, pp. 898–904. DOI: 10.1016/j.icarus.2013.06.033.

Běhounková, M. et al. (2015). "Timing of water plume eruptions on Enceladus explained by interior viscosity structure". In: *Nat. Geosci.* 8, pp. 601–604. DOI: 10.1038/ngeo2475.

Běhounková, M., M. Beuthe, and O. Souček (2018). "Benchmark for tidal deformation in planetary shells of variable thickness". In: *European Planetary Science Congress*, EPSC2018–427.

Běhounková, M., G. Tobie, G. Choblet, and O. Čadek (2012). "Tidally-induced melting events as the origin of south-pole activity on Enceladus". In: *Icarus* 219, pp. 655–664. DOI: 10.1016/j.icarus.2012.03.024.

Běhounková, M., G. Tobie, G. Choblet, and O. Čadek (2010). "Coupling mantle convection and tidal dissipation: Applications to Enceladus and Earth-like planets". In: *J. Geophys. Res. Planets* 115.E9, E09011. DOI: 10.1029/2009JE003564.

Běhounková, M., G. Tobie, G. Choblet, and O. Čadek (2011). "Tidally induced thermal runaways on extrasolar Earths: impact on habitability". In: *Astrophys. J.* 728.2, 89. DOI: 10.1088/0004-637X/728/2/89.

Běhounková, M. et al. (2021). "Tidally Induced Magmatic Pulses on the Oceanic Floor of Jupiter's Moon Europa". In: *Geophys. Res. Let.* 48.3, e2020GL090077. DOI: 10.1029/2020GL090077.

Beuthe, M. (2013). "Spatial patterns of tidal heating". In: *Icarus* 223.1, pp. 308–329. DOI: 10.1016/j.icarus.2012.11.020.

Beuthe, M. (2016). "Crustal control of dissipative ocean tides in Enceladus and other icy moons". In: *Icarus* 280, pp. 278–299. DOI: 10.1016/j.icarus.2016.08.009.

Beuthe, M., A. Rivoldini, and A. Trinh (2016). "Enceladus's and Dione's floating ice shells supported by minimum stress isostasy". In: *Geophys. Res. Let.* 43, pp. 10088–10096. DOI: 10.1002/2016GL070650.

Beuthe, M. (2015a). "Tidal Love numbers of membrane worlds: Europa, Titan, and Co." In: *Icarus* 258, pp. 239–266. DOI: 10.1016/j.icarus.2015.06.008.

Beuthe, M. (2015b). "Tides on Europa: The membrane paradigm". In: *Icarus* 248, pp. 109–134. DOI: 10.1016/j.icarus.2014.10.027.

Beuthe, M. (2018). "Enceladus's crust as a non-uniform thin shell: I tidal deformations". In: *Icarus* 302, pp. 145–174. DOI: 10.1016/j.icarus.2017.11.009.

Beuthe, M. (2019). "Enceladus's crust as a non-uniform thin shell: II tidal dissipation". In: *Icarus* 332, pp. 66–91. DOI: 10.1016/j.icarus.2019.05.035.

Bierhaus, E. B., K. Zahnle, and C. R. Chapman (2009). "Europa's Crater Distributions and Surface Ages". In: *Europa*. Ed. by R. T. Pappalardo, W. B. McKinnon, and K. K. Khurana. Univ. Ariz. Press, pp. 161–.

Bierson, C. and F. Nimmo (2016). "A test for Io's magma ocean: Modeling tidal dissipation with a partially molten mantle". In: *J. Geophys. Res. Planets* 121.11, pp. 2211–2224. DOI: 10.1002/2016JE005005.

Bills, B. G., G. A. Neumann, D. E. Smith, and M. T. Zuber (2005). "Improved estimate of tidal dissipation within Mars from MOLA observations of the shadow of Phobos". In: *J. Geophys. Res. Planets* 110.E7, E07004. DOI: 10.1029/2004JE002376.

Bland, M., A. Showman, and G. Tobie (2008). "The production of Ganymede's magnetic field". In: *Icarus* 198, pp. 384–399. DOI: 10.1016/j.icarus.2008.07.011.

Bolmont, E. et al. (2020). "Impact of tides on the transit-timing fits to the TRAPPIST-1 system". In: *Astronomy & Astrophysics* 635, A117. DOI: 10.1051/0004-6361/202037546.

Budd, W. and T. Jacka (1989). "A review of ice rheology for ice-sheet modeling". In: *Cold regions science and technology* 16, pp. 107–144. DOI: 10.1016/0165-232X(89)90014-1.

Burša, M. and K. Pěč (1988). *Tíhové pole a dynamika Země*. První vydání. Praha: Academia.

Čadek, O. et al. (2016). "Enceladus's internal ocean and ice shell constrained from Cassini gravity, shape, and libration data". In: *Geophys. Res. Let.* 46, pp. 5653–5660. DOI: 10.1002/2016GL068634.

Čadek, O. et al. (2019). "Long-term stability of Enceladus' uneven ice shell". In: *Icarus* 319, pp. 476–484. DOI: 10.1016/j.icarus.2018.10.003.

Cassidy, T. et al. (2013). "Magnetospheric ion sputtering and water ice grain size at Europa". In: *Plan. Space Sci.* 77, pp. 64–73. DOI: 10.1016/j.pss.2012.07.008.

Castillo-Rogez, J. C., M. Efroimsky, and V. Lainey (2011). "The tidal history of Iapetus: Spin dynamics in the light of a refined dissipation model". In: *J. Geophys. Res. Planets* 116.E9, E09008. DOI: 10.1029/2010JE003664.

Choblet, G. (2005). "Modelling thermal convection with large viscosity gradients in one block of the 'cubed sphere'". In: *J. Comput. Phys.* 205, pp. 269–291. DOI: 10.1016/j.jcp.2004.11.005.

Choblet, G., O. Čadek, F. Couturier, and C. Dumoulin (2007). "ŒDIPUS: A new tool to study the dynamics of planetary interiors". In: *Geophys. J. Int.* 170, pp. 9–30. DOI: 10.1111/j.1365-246X.2007.03419.x.

Choblet, G. et al. (2017). "Powering prolonged hydrothermal activity inside Enceladus". In: *Nat. Astron.* 1, pp. 841–847. DOI: 10.1038/s41550-017-0289-8.

Collins, G. C. and J. C. Goodman (2007). "Enceladus' south polar sea". In: *Icarus* 189, pp. 72–82. DOI: 10.1016/j.icarus.2007.01.010.

Correia, A. C. M., G. Boué, J. Laskar, and A. Rodriguez (2014). "Deformation and tidal evolution of close-in planets and satellites using a Maxwell viscoelastic rheology". In: *Astronomy & Astrophysics* 571, A50. DOI: 10.1051/0004-6361/201424211.

Correia, A. C. M. and J. Laskar (2009). "Mercury's capture into the 3/2 spin-orbit resonance including the effect of core-mantle friction". In: *Icarus* 201.1, pp. 1–11. DOI: 10.1016/j.icarus.2008.12.034.

Crow-Willard, E. N. and R. T. Pappalardo (2015). "Structural mapping of Enceladus and implications for formation of tectonized regions". In: *J. Geophys. Res.* 120, pp. 928–950. DOI: 10.1002/2015JE004818.

Csizmadia, S., H. Hellard, and A. M. S. Smith (2019). "An estimate of the k_2 Love number of WASP-18Ab from its radial velocity measurements". In: *Astronomy & Astrophysics* 623, A45. DOI: 10.1051/0004-6361/201834376.

Ćuk, M., L. Dones, and D. Nesvorný (2016). "Dynamical evidence for a late formation of Saturn's moons". In: *Astrophys. J.* 820.2, 97. DOI: 10.3847/0004-637X/820/2/97.

Davaille, A. and C. Jaupart (1994). "Onset of thermal convection in fluids with temperature-dependent viscosity — applications to the oceanic mantle". In: *J. Geophys. Res.* 99.B10, pp. 19, 853–19, 866. DOI: 10.1029/94JB01405.

Dirkx, D. et al. (2017). "On the contribution of PRIDE-JUICE to Jovian system ephemerides". In: *Plan. Space Sci.* 147, pp. 14–27. DOI: 10.1016/j.pss.2017.09.004.

Dobos, V., R. Heller, and E. L. Turner (2017). "The effect of multiple heat sources on exomoon habitable zones". In: *Astronomy & Astrophysics* 601.A91, p. 7. DOI: 10.1051/0004-6361/201730541.

Dobrovolskis, A. R. (2007). "Spin states and climates of eccentric exoplanets". In: *Icarus* 192.1, pp. 1–23. DOI: 10.1016/j.icarus.2007.07.005.

Dobrovolskis, A. R. (2013). "Insolation on exoplanets with eccentricity and obliquity". In: *Icarus* 226.1, pp. 760–776. DOI: 10.1016/j.icarus.2013.06.026.

Driscoll, P. E. and R. Barnes (2015). "Tidal Heating of Earth-like Exoplanets around M Stars: Thermal, Magnetic, and Orbital Evolutions". In: *Astrobiology* 15.9, pp. 739–760. DOI: 10.1089/ast.2015.1325.

Dumoulin, C., G. Tobie, O. Verhoeven, P. Rosenblatt, and N. Rambaux (2017). "Tidal constraints on the interior of Venus". In: *J. Geophys. Res. Planets* 122.6, pp. 1338–1352. DOI: 10.1002/2016JE005249.

Durham, W. B., L. A. Stern, and S. H. Kirby (2001). "Rheology of ice I at low stress and elevated confining pressure". In: *J. Geophys. Res.* 106, pp. 11031–11042. DOI: 10.1029/2000JB900446.

Dvorak, R., E. Pilat-Lohinger, E. Bois, and *et al.* (2010). "Dynamical Habitability of Planetary Systems". In: *Astrobiology* 10, pp. 33–43. DOI: 10.1089/ast.2009.0379.

Efroimsky, M. (2012). "Tidal Dissipation Compared to Seismic Dissipation: In Small Bodies, Earths, and Super-Earths". In: *Astrophys. J.* 746, 150. DOI: 10.1088/0004-637X/746/2/150.

Efroimsky, M. and V. Lainey (2007). "Physics of bodily tides in terrestrial planets and the appropriate scales of dynamical evolution". In: *J. Geophys. Res. Planets* 112.E12, E12003. DOI: 10.1029/2007JE002908.

Efroimsky, M. and V. V. Makarov (2014). "Tidal Dissipation in a Homogeneous Spherical Body. I. Methods". In: *Astrophys. J.* 795.1, 6. DOI: 10.1088/0004-637X/795/1/6.

Efroimsky, M. and J. G. Williams (2009). "Tidal torques. A critical review of some techniques". In: *Celest. Mech. Dyn. A.* 104.3, pp. 257–289. DOI: 10.1007/s10569-009-9204-7.

Ermakov, A. I. et al. (2020). "A Recipe for Geophysical Exploration of Enceladus". In: *arXiv*, 2008.02887.

Ferraz-Mello, S. (2015). "Tidal synchronization of close-in satellites and exoplanets: II. Spin dynamics and extension to Mercury and exoplanet host stars". In: *Celest. Mech. Dyn. A.* 122.4, pp. 359–389. DOI: 10.1007/s10569-015-9624-5.

Figueredo, P. H. and R. Greeley (2004). "Resurfacing history of Europa from pole-to-pole geological mapping". In: *Icarus* 167.2, pp. 287–312. DOI: 10.1016/j.icarus.2003.09.016.

Fischer, H.-J. and T. Spohn (1990). "Thermal-orbital histories of viscoelastic models of Io (J1)". In: *Icarus* 83.1, pp. 39–65. DOI: 10.1016/0019-1035(90)90005-T.

Fuller, J., J. Luan, and E. Quataert (2016). "Resonance locking as the source of rapid tidal migration in the Jupiter and Saturn moon systems". In: *Mon. Not. R. Astron. Soc.* 458, 3867. DOI: 10.1093/mnras/stw609.

Gerya, T. (2010). *Introduction to Numerical Geodynamic Modelling.* Cambridge University Press.

Goldsby, D. and D. Kohlstedt (2001). "Superplastic deformation of ice: Experimental observations". In: *J. Geophys. Res.* 106, pp. 11017–11030. DOI: 10.1029/2000JB900336.

Gomez Casajus, L. et al. (2021). "Updated Europa gravity field and interior structure from a reanalysis of Galileo tracking data". In: *Icarus* 358, 114187. DOI: 10.1016/j.icarus.2020.114187.

Grasset, O. et al. (2013). "JUpiter ICy moons Explorer (JUICE): An ESA mission to orbit Ganymede and to characterise the Jupiter system". In: *Plan. Space Sci.* 78, pp. 1–21. DOI: 10.1016/j.pss.2012.12.002.

Gribb, T. and R. Cooper (1998). "Low-frequency shear attenuation in polycrystalline olivine: Grain boundary diffusion and the physical significance of the Andrade model for viscoelastic rheology". In: *J. Geophys. Res. Solid Earth* 103.B11, pp. 27267–27279. DOI: 10.1029/98JB02786.

Han, L., G. Tobie, and A. P. Showman (2012). "The impact of a weak south pole on thermal convection in Enceladus' ice shell". In: *Icarus* 218, pp. 320–330. DOI: 10.1016/j.icarus.2011.12.006.

Hansen, C. J. et al. (2006). "Enceladus' Water Vapor Plume". In: *Science* 311.5766, pp. 1422–1425. DOI: 10.1126/science.1121254.

Hedman, M. M. et al. (2013). "An observed correlation between plume activity and tidal stresses on Enceladus". In: *Nature* 500, pp. 182–184. DOI: 10.1038/nature12371.

Hellard, H., S. Csizmadia, S. Padovan, F. Sohl, and H. Rauer (2020). "HST/STIS Capability for Love Number Measurement of WASP-121b". In: *Astrophys. J.* 889.1, 66. DOI: 10.3847/1538-4357/ab616e.

Hellard, H. et al. (2019). "Retrieval of the Fluid Love Number k $_2$ in Exoplanetary Transit Curves". In: *Astrophys. J.* 878.2, 119. DOI: 10.3847/1538-4357/ab2048.

Heller, R. and R. Barnes (2013). "Exomoon Habitability Constrained by Illumination and Tidal Heating". In: *Astrobiology* 13.1, pp. 18–46. DOI: 10.1089/ast.2012.0859.

Hemingway, D. J., L. Iess, R. Tajeddine, and G. Tobie (2018). "The interior of Enceladus". In: *Enceladus and the Icy Moons of Saturn.* Ed. by Schenk, Paul M. and Clark, Roger N. and Howett Carly J. A. and Verbiscer, Anne J. and Waite, J. Hunter. Tucson: Univ. of Arizona, pp. 57–77. DOI: 10.2458/azu_uapress_9780816537075-ch004.

Henning, W. G. and T. Hurford (2014). "Tidal Heating in Multilayered Terrestrial Exoplanets". In: *Astrophys. J.* 789.1, 30. DOI: 10.1088/0004-637X/789/1/30.

Henning, W. G., R. J. O'Connell, and D. D. Sasselov (2009). "Tidally Heated Terrestrial Exoplanets: Viscoelastic Response Models". In: *Astrophys. J.* 707.2, pp. 1000–1015. DOI: 10.1088/0004-637X/707/2/1000.

Henning, W. G. et al. (2018). "Highly Volcanic Exoplanets, Lava Worlds, and Magma Ocean Worlds: An Emerging Class of Dynamic Exoplanets of Significant Scientific Priority". In: *arXiv*, 1804.05110.

Howell, S. M. and R. T. Pappalardo (2020). "NASA's Europa Clipper–a mission to a potentially habitable ocean world". In: *Nat. Commun.* 11 (1), p. 1311. DOI: 10.1038/s41467-020-15160-9.

Howell, S. M. et al. (2020). "Ocean Worlds Exploration and the Search for Life". In: *arXiv*, 2006.15803.

Howett, C. J. A., J. R. Spencer, J. Pearl, and M. Segura (2011). "High heat flow from Enceladus' south polar region measured using 10-600 cm^{-1} Cassini/CIRS data". In: *J. Geophys. Res. Planets* 116.15, E03003. DOI: 10.1029/2010JE003718.

Hsu, H.-W. et al. (2015). "Ongoing hydrothermal activities within Enceladus". In: *Nature* 519, pp. 207–210. DOI: 10.1038/nature14262.

Hurford, T. A., P. Helfenstein, G. V. Hoppa, R. Greenberg, and B. G. Bills (2007). "Eruptions arising from tidally controlled periodic openings of rifts on Enceladus". In: *Nature* 447, pp. 292–294. DOI: 10.1038/nature05821.

Hussmann, H. and T. Spohn (2004). "Thermal-orbital evolution of Io and Europa". In: *Icarus* 171, pp. 391–410. DOI: 10.1016/j.icarus.2004.05.020.

Hussmann, H., T. Spohn, and K. Wieczerkowski (2002). "Thermal equilibrium states of Europa's ice shell: Implications for internal ocean thickness and surface heat flow". In: *Icarus* 156, pp. 143–151. DOI: 10.1006/icar.2001.6776.

Hussmann, H. et al. (2010). "Implications of Rotation, Orbital States, Energy Sources, and Heat Transport for Internal Processes in Icy Satellites". In: *Space Science Rev.* 153, pp. 317–348. DOI: 10.1007/s11214-010-9636-0.

Iess, L. et al. (2014). "The Gravity Field and Interior Structure of Enceladus". In: *Science* 344.6179, pp. 78–80. DOI: 10.1126/science.1250551.

Ingersoll, A. P. and S. P. Ewald (2017). "Decadal timescale variability of the Enceladus plumes inferred from Cassini images". In: *Icarus* 282, pp. 260–275. DOI: 10.1016/j.icarus.2016.09.018.

Ingersoll, A. P., S. P. Ewald, and S. K. Trumbo (2020). "Time variability of the Enceladus plumes: Orbital periods, decadal periods, and aperiodic change". In: *Icarus* 344, 113345. DOI: 10.1016/j.icarus.2019.06.006.

Jackson, I. (2015). "2.21 - Properties of Rocks and Minerals: Physical Origins of Anelasticity and Attenuation in Rock". In: *Treatise on Geophysics (Second Edi-*

tion). Ed. by G. Schubert. Second Edition. Oxford: Elsevier, pp. 539–571. DOI: https://doi.org/10.1016/B978-0-444-53802-4.00045-2.

Jackson, I., J. Fitz Gerald, U. Faul, and B. Tan (2002). "Grain-size-sensitive seismic wave attenuation in polycrystalline olivine". In: *J. Geophys. Res. Solid Earth* 107.B12, 2360. DOI: 10.1029/2001JB001225.

Jara-Orué, H. M. and B. L. Vermeersen (2011). "Effects of low-viscous layers and a non-zero obliquity on surface stresses induced by diurnal tides and non-synchronous rotation: The case of Europa". In: *Icarus* 215.1, pp. 417–438. DOI: https://doi.org/10.1016/j.icarus.2011.05.034.

Kaltenegger, L., W. G. Henning, and D. D. Sasselov (2010). "Detecting volcanism on extrasolar planets". In: *Astronomical J.* 140.5, pp. 1370–1380. DOI: 10.1088/0004-6256/140/5/1370.

Kang, W. et al. (2020). "Differing Enceladean ocean circulation and ice shell geometries driven by tidal heating in the ice versus the core". In: *arXiv*, 2008.03764.

Karato, S.-I. (2012). *Deformation of Earth materials: an introduction to the rheology of solid Earth*. Cambridge University Press.

Kasting, J. F., D. P. Whitmire, and R. T. Reynolds (1993). "Habitable Zones around Main Sequence Stars". In: *Icarus* 101, pp. 108–128. DOI: 10.1006/icar.1993.1010.

Kattenhorn, S. A. and L. M. Prockter (2014). "Evidence for subduction in the ice shell of Europa". In: *Nature Geoscience* 7.10, pp. 762–767. DOI: 10.1038/ngeo2245.

Kaula, W. M. (1961). "Analysis of Gravitational and Geometric Aspects of Geodetic Utilization of Satellites". In: *Geophys. J. R. Astron. Soc.* 5.2, pp. 104–133. DOI: 10.1111/j.1365-246X.1961.tb00417.x.

Kaula, W. M. (1964). "Tidal dissipation by solid friction and the resulting orbital evolution". In: *Rev. Geophys.* 2.4, pp. 661–685. DOI: 10.1029/RG002i004p00661.

Kervazo, M., G. Tobie, G. Choblet, C. Dumoulin, and M. Běhounková (2021). "Solid tides in Io's partially molten interior. Contribution of bulk dissipation". In: *Astronomy & Astrophysics* 650, A72. DOI: 10.1051/0004-6361/202039433.

Kervazo, M., G. Tobie, G. Choblet, C. Dumoulin, and M. Běhounková (sub). "Inferring Io's interior from tidal monitoring". In: *Icarus* 123.

Khan, A. et al. (2018). "A Geophysical Perspective on the Bulk Composition of Mars". In: *J. Geophys. Res. Planets* 123.2, pp. 575–611. DOI: https://doi.org/10.1002/2017JE005371.

King, S. D. et al. (2010). "A community benchmark for 2-D Cartesian compressible convection in the Earth's mantle". In: *Geophys. J. Int.* 180.1, pp. 73–87. DOI: 10.1111/j.1365-246X.2009.04413.x.

Kite, E. S., E. Gaidos, and M. Manga (2011). "Climate Instability on Tidally Locked Exoplanets". In: *Astrophys. J.* 743.1, 41. DOI: 10.1088/0004-637X/743/1/41.

Kite, E. S. and A. M. Rubin (2016). "Sustained eruptions on Enceladus explained by turbulent dissipation in tiger stripes". In: *Proc. Natl. Acad. Sci. U.S.A.* 113, pp. 3972–3975. DOI: 10.1073/pnas.1520507113.

Kivelson, M. G. et al. (2000). "Galileo magnetometer measurements: A stronger case for a subsurface ocean at Europa". In: *Science* 289.5483, pp. 1340–1343. DOI: 10.1126/science.289.5483.1340.

Kreidberg, L. et al. (2019). "Absence of a thick atmosphere on the terrestrial exoplanet LHS 3844b". In: *Nature* 573.7772, pp. 87–90. DOI: 10.1038/s41586-019-1497-4.

Lainey, V. et al. (2012). "Strong Tidal Dissipation in Saturn and Constraints on Enceladus' Thermal State from Astrometry". In: *Astrophys. J.* 752, 14. DOI: 10.1088/0004-637X/752/1/14.

Lainey, V. (2016). "Quantification of tidal parameters from Solar System data". In: *Celest. Mech. Dyn. A.* 126.1-3, pp. 145–156. DOI: 10.1007/s10569-016-9695-y.

Lainey, V., J.-E. Arlot, Ö. Karatekin, and T. Van Hoolst (2009). "Strong tidal dissipation in Io and Jupiter from astrometric observations". In: *Nature* 459.7249, pp. 957–959. DOI: 10.1038/nature08108.

Lammer, H., F. Selsis, E. Chassefière, and *et al.* (2010). "Geophysical and Atmospheric Evolution of Habitable Planets". In: *Astrobiology* 10, pp. 45–68. DOI: 10.1089/ast.2009.0368.

Leonard, E., R. Pappalardo, and A. Yin (2018). "Analysis of very-high-resolution Galileo images and implications for resurfacing mechanisms on Europa". In: *Icarus* 312, pp. 100–120. DOI: 10.1016/j.icarus.2018.04.016.

Liao, Y., F. Nimmo, and J. A. Neufeld (2020). "Heat Production and Tidally Driven Fluid Flow in the Permeable Core of Enceladus". In: *J. Geophys. Res. Planets* 125.9, e2019JE006209. DOI: 10.1029/2019JE006209.

Lopes, R. and D. Williams (2005). "Io after Galileo". In: *Rep. Prog. Phys.* 68, pp. 303–340. DOI: 10.1088/0034-4885/68/2/R02.

Love, A. E. H. (1907). *Lehrbuch der Elastizität.*

Makarov, V. V. (2015). "Equilibrium Rotation of Semiliquid Exoplanets and Satellites". In: *Astrophys. J.* 810.1, 12. DOI: 10.1088/0004-637X/810/1/12.

Makarov, V. V., C. T. Berghea, and M. Efroimsky (2018). "Spin-orbital Tidal Dynamics and Tidal Heating in the TRAPPIST-1 Multiplanet System". In: *Astrophys. J.* 857.2, 14. DOI: 10.3847/1538-4357/aab845.

Makarov, V. V. and M. Efroimsky (2013). "No Pseudosynchronous Rotation for Terrestrial Planets and Moons". In: *Astrophys. J.* 764.1, 27. DOI: 10.1088/0004-637X/764/1/27.

Martinec, Z. (1989). "Program to calculate the spectral harmonic expansion coefficients of the 2 scalar fields product". In: *Comput. Phys. Commun.* 54, pp. 177–182. DOI: 10.1016/0010-4655(89)90043-X.

Martinec, Z. (2019). *Principles of Continuum Mechanics: A Basic Course for Physicists*. Nečas Center Series. Springer International Publishing.

Martinec, Z., C. Matyska, E. W. Grafarend, and P. Vaníček (1993). "Helmert's 2nd condensation method". In: *Manuscr. Geod.* 18, pp. 417–421.

Marusiak, A. G. et al. (2021). "Exploration of Icy Ocean Worlds Using Geophysical Approaches". In: *Planet. Sci. J.* 2.4, 150. DOI: 10.3847/psj/ac1272.

Matsuyama, I., M. Beuthe, H. C. F. C. Hay, F. Nimmo, and S. Kamata (2018). "Ocean tidal heating in icy satellites with solid shells". In: *Icarus* 312, pp. 208–230. DOI: 10.1016/j.icarus.2018.04.013.

McKinnon, W. B. (2015). "Effect of Enceladus's rapid synchronous spin on interpretation of Cassini gravity". In: *Geophys. Res. Let.* 42, pp. 2137–2143. DOI: 10.1002/2015GL063384.

Meier, T. G., D. J. Bower, T. Lichtenberg, P. J. Tackley, and B.-O. Demory (2021). "Hemispheric Tectonics on LHS 3844b". In: *Astrophys. J. Let.* 908.2, L48. DOI: 10.3847/2041-8213/abe400.

Meyer, J. and J. Wisdom (2007). "Tidal heating in Enceladus". In: *Icarus* 188, pp. 535–539. DOI: 10.1016/j.icarus.2007.03.001.

Meyer, J. and J. Wisdom (2008). "Episodic volcanism on Enceladus: Application of the Ojakangas Stevenson model". In: *Icarus* 198.1, pp. 178–180. DOI: 10.1016/j.icarus.2008.06.012.

Mignard, F. (1979). "The Evolution of the Lunar Orbit Revisited. I." In: *Moon and Planets* 20.3, pp. 301–315. DOI: 10.1007/BF00907581.

Mitri, G. and A. P. Showman (2008). "Thermal convection in ice-I shells of Titan and Enceladus". In: *Icarus* 193, pp. 387–396. DOI: 10.1016/j.icarus.2007.07.016.

Moore, W. B. (2003). "Tidal heating and convection in Io". In: *J. Geophys. Res. Planets* 108.E8, 5096. DOI: 10.1029/2002JE001943.

Moore, W. B., J. I. Simon, and A. A. G. Webb (2017). "Heat-pipe planets". In: *Earth Plan. Sci. Let.* 474, pp. 13–19. DOI: 10.1016/j.epsl.2017.06.015.

Murray, C. D. and S. F. Dermott (1999). *Solar system dynamics*. Cambridge: Cambridge University Press.

Nahm, A. L. and S. A. Kattenhorn (2015). "A unified nomenclature for tectonic structures on the surface of Enceladus". In: *Icarus* 258, pp. 67–81. DOI: 10.1016/j.icarus.2015.06.009.

Neveu, M. and A. R. Rhoden (2019). "Evolution of Saturn's mid-sized moons". In: *Nat. Astron.* 3, pp. 543–552. DOI: 10.1038/s41550-019-0726-y.

Neveu, M. et al. (2020). "Returning Samples from Enceladus for Life Detection". In: *Front. Astron. Space Sci.* 7, 26. DOI: 10.3389/fspas.2020.00026.

Nimmo, F. and R. T. Pappalardo (2006). "Diapir-induced reorientation of Saturn's moon Enceladus". In: *Nature* 441, pp. 614–616. DOI: 10.1038/nature04821.

Nimmo, F., C. Porco, and C. Mitchell (2014). "Tidally Modulated Eruptions on Enceladus: Cassini ISS Observations and Models". In: *Astronomical J.* 148, 46. DOI: 10.1088/0004-6256/148/3/46.

O'Neill, C. and F. Nimmo (2010). "The role of episodic overturn in generating the surface geology and heat flow on Enceladus". In: *Nat. Geosci.* 3, pp. 88–91. DOI: 10.1038/ngeo731.

Ojakangas, G. W. and D. J. Stevenson (1986). "Episodic volcanism of tidally heated satellites with application to Io". In: *Icarus* 66.2, pp. 341–358. DOI: 10.1016/0019-1035(86)90163-6.

Ojakangas, W. and D. Stevenson (1989). "Thermal state of an ice shell on Europa". In: *Icarus* 81.2, pp. 220–241. DOI: 10.1016/0019-1035(89)90052-3.

Parmentier, E., C. Sotin, and B. Travis (1994). "Turbulent 3-D thermal convection in an infinite Prandtl number, volumetrically heated fluid: implications for mantle dynamics". In: *Geophys. J. Int.* 116, pp. 241–251. DOI: 10.1111/j.1365-246X.1994.tb01795.x.

Peale, S. J. and T. Gold (1965). "Rotation of the Planet Mercury". In: *Nature* 206.4990, pp. 1240–1241. DOI: 10.1038/2061240b0.

Pleiner Sládková, K., O. Souček, and M. Běhounková (sub). "Enceladus' tiger stripes as frictional faults: Effect on stress and heat production". In: *Geophys. Res. Let.* DOI: 10.1029/2021GL094849.

Porco, C., D. DiNino, and F. Nimmo (2014). "How the Geysers, Tidal Stresses, and Thermal Emission across the South Polar Terrain of Enceladus are Related". In: *Astronomical J.* 148, 45. DOI: 10.1088/0004-6256/148/3/45.

Porco, C. et al. (2006). "Cassini observes the active south pole of Enceladus". In: *Science* 311, pp. 1393–1401. DOI: 10.1126/science.1123013.

Postberg, F., J. Schmidt, J. Hillier, S. Kempf, and R. Srama (2011). "A salt-water reservoir as the source of a compositionally stratified plume on Enceladus". In: *Nature* 474, pp. 620–622. DOI: 10.1038/nature10175.

Postberg, F. et al. (2009). "Sodium salts in E-ring ice grains from an ocean below the surface of Enceladus". In: *Nature* 459, pp. 1098–1101. DOI: 10.1038/nature08046.

Press, W. H., S. A. Teukolsky, W. T. Vetterling, and B. P. Flannery (1992). *Numerical recipes in FORTRAN: the art of scientific computing*. Second. Cambridge University Press.

Ralston, A. (1965). *A First Course in Numerical Analysis*. New York: McGraw-Hill.

Renaud, J. P. and W. G. Henning (2018). "Increased Tidal Dissipation Using Advanced Rheological Models: Implications for Io and Tidally Active Exoplanets". In: *Astrophys. J.* 857.2, 98. DOI: 10.3847/1538-4357/aab784.

Renaud, J. P. et al. (2021). "Tidal Dissipation in Dual-body, Highly Eccentric, and Nonsynchronously Rotating Systems: Applications to Pluto-Charon and the Exoplanet TRAPPIST-1e". In: *Planet. Sci. J.* 2.1, 4. DOI: 10.3847/PSJ/abc0f3.

Rhoden, A. R. et al. (2010). "Constraints on Europa's rotational dynamics from modeling of tidally-driven fractures". In: *Icarus* 210.2, pp. 770–784. DOI: 10.1016/j.icarus.2010.07.018.

Rhoden, A. R. et al. (2020). "The formation of Enceladus' Tiger Stripe Fractures from eccentricity tides". In: *Earth Plan. Sci. Let.* 544, 116389. DOI: 10.1016/j.epsl.2020.116389.

Rivoldini, A., T. Van Hoolst, O. Verhoeven, A. Mocquet, and V. Dehant (2011). "Geodesy constraints on the interior structure and composition of Mars". In: *Icarus* 213.2, pp. 451–472. DOI: 10.1016/j.icarus.2011.03.024.

Roberts, J. H. (2015). "The fluffy core of Enceladus". In: *Icarus* 258, pp. 54–66. DOI: 10.1016/j.icarus.2015.05.033.

Roberts, J. and F. Nimmo (2008). "Tidal heating and the long-term stability of a subsurface ocean on Enceladus". In: *Icarus* 194, pp. 675–689. DOI: 10.1016/j.icarus.2007.11.010.

Ronchi, C., R. Iacono, and P. S. Paolucci (1996). "The "cubed sphere": a new method for the solution of partial differential equations in spherical geometry". In: *J. Comput. Phys.* 124.1, pp. 93–114. DOI: 10.1006/jcph.1996.0047.

Rovira-Navarro, M. et al. (2019). "Do tidally-generated inertial waves heat the subsurface oceans of Europa and Enceladus?" In: *Icarus* 321, pp. 126–140. DOI: 10.1016/j.icarus.2018.11.010.

Sabadini, R. and B. Vermeersen (2004). *Global Dynamics of the Earth: Applications of Normal Mode Relaxation Theory to Solid-Earth Geophysics*. Dodrech, the Netherlands: Kluwer Academic Publishers.

Samuel, H., P. Lognonné, M. Panning, and V. Lainey (2019). "The rheology and thermal history of Mars revealed by the orbital evolution of Phobos". In: *Nature* 569.7757, pp. 523–527. DOI: 10.1038/s41586-019-1202-7.

Shoji, D., H. Hussmann, K. Kurita, and F. Sohl (2013). "Ice rheology and tidal heating of Enceladus". In: *Icarus* 226, pp. 10–19. DOI: 10.1016/j.icarus.2013.05.004.

Shoji, D. and K. Kurita (2014). "Thermal-Orbital Coupled Tidal Heating and Habitability of Martian-sized Extrasolar Planets around M Stars". In: *Astrophys. J.* 789.1, 3. DOI: 10.1088/0004-637X/789/1/3.

Showman, A. P., D. J. Stevenson, and R. Malhotra (1997). "Coupled orbital and thermal evolution of Ganymede". In: *Icarus* 129, pp. 367–383. DOI: 10.1006/icar.1997.5778.

Sládková, K., O. Souček, K. Kalousová, and M. Běhounková (2020). "Tidal Walking on Europa's Strike-Slip Faults-Insight From Numerical Modeling". In: *J. Geophys. Res. Planets* 125.8, e2019JE006327. DOI: 10.1029/2019JE006327.

Solomatov, V. S. (1995). "Scaling of temperature- and stress-dependent viscosity convection". In: *Phys. Fluids.* 7.2, pp. 266–274. DOI: 10.1063/1.868624.

Solomatov, V. and A. Barr (2006). "Onset of convection in fluids with strongly temperature-dependent, power-law viscosity". In: *Phys. Earth Planet. Inter.* 155, pp. 140–145. DOI: /10.1016/j.pepi.2005.11.001.

Souček, O., J. Hron, M. Běhounková, and O. Čadek (2016). "Effect of the tiger stripes on the deformation of Saturn's moon Enceladus". In: *Geophys. Res. Let.* 43.14, pp. 7417–7423. DOI: 10.1002/2016GL069415.

Souček, O. et al. (2019). "Tidal dissipation in Enceladus' uneven, fractured ice shell". In: *Icarus* 328, pp. 218–231. DOI: 10.1016/j.icarus.2019.02.012.

Spencer, D. C., R. F. Katz, and I. J. Hewitt (2020). "Magmatic intrusions control Io's crustal thickness". In: *J. Geophys. Res. Planets* 125.6, e2020JE006443. DOI: 10.1029/2020JE006443.

Spencer, D. C., R. F. Katz, and I. J. Hewitt (2021). "Tidal controls on the lithospheric thickness and topography of Io from magmatic segregation and volcanism modelling". In: *Icarus*, 114352. DOI: 10.1016/j.icarus.2021.114352.

Spencer, J. R., J. C. Pearl, M. Segura, F. M. Flasar, and et al. (2006). "Cassini encounters Enceladus: Background and the discovery of a south polar hot spot". In: *Science* 311, pp. 1401–1405. DOI: 10.1126/science.1121661.

Spencer, J. R. et al. (2018). "Plume Origins and Plumbing: From Ocean To Surface". In: *Enceladus and the Icy Moons of Saturn.* Ed. by Schenk, Paul M. and Clark, Roger N. and Howett Carly J. A. and Verbiscer, Anne J. and Waite, J. Hunter.

Tucson: University of Arizona, pp. 163–174. DOI: 10.2458/azu_uapress_9780816537075-ch008.

Stegman, D. R., J. Freeman, and D. A. May (2009). "Origin of ice diapirism, true polar wander, subsurface ocean, and tiger stripes of Enceladus driven by compositional convection". In: *Icarus* 202, pp. 669–680. DOI: 10.1016/j.icarus.2009.03.017.

Steinke, T., H. Hu, D. Höning, W. van der Wal, and B. Vermeersen (2020). "Tidally induced lateral variations of Io's interior". In: *Icarus* 335, 113299. DOI: 10.1016/j.icarus.2019.05.001.

Summeren, J. van, C. P. Conrad, and E. Gaidos (2011). "Mantle convection, plate tectonics, and volcanism on hot exo-Earths". In: *Astrophys. J. Let.* 736, L15. DOI: 10.1088/2041-8205/736/L15.

Sundberg, M. and R. F. Cooper (2010). "A composite viscoelastic model for incorporating grain boundary sliding and transient diffusion creep; correlating creep and attenuation responses for materials with a fine grain size". In: *Philos. Mag.* 90.20, pp. 2817–2840. DOI: 10.1080/14786431003746656.

Tackley, P. (2008). "Modelling compressible mantle convection with large viscosity contrasts in a three-dimensional spherical shell using the yin-yang grid". In: *Phys. Earth Planet. Inter.* 171, pp. 7–18. DOI: doi:10.1016/j.pepi.2008.08.005.

Takeuchi, H. and M. Saito (1972). "Seismic Surface Waves". In: *Methods in Computational Physics: Advances in Research and Applications* 11, pp. 217–295. DOI: 10.1016/B978-0-12-460811-5.50010-6.

Taylor, P. A. and J.-L. Margot (2010). "Tidal evolution of close binary asteroid systems". In: *Celest. Mech. Dyn. A.* 108.4, pp. 315–338. DOI: 10.1007/s10569-010-9308-0.

Thomas, P. C. et al. (2007). "Shapes of the saturnian icy satellites and their significance". In: *Icarus* 190, pp. 573–584. DOI: 10.1016/j.icarus.2007.03.012.

Thomas, P. C. et al. (2016). "Enceladus's measured physical libration requires a global subsurface ocean". In: *Icarus* 264, pp. 37–47. DOI: 10.1016/j.icarus.2015.08.037.

Tobie, G., A. Mocquet, and C. Sotin (2005). "Tidal dissipation within large icy satellites: Applications to Europa and Titan". In: *Icarus* 177.2, pp. 534–549. DOI: 10.1016/j.icarus.2005.04.006.

Tobie, G., O. Čadek, and C. Sotin (2008). "Solid tidal friction above a liquid water reservoir as the origin of the South Pole Hotspot on Enceladus". In: *Icarus* 196.2, pp. 642–652. DOI: 10.1016/j.icarus.2008.03.008.

Tobie, G., O. Grasset, C. Dumoulin, and A. Mocquet (2019). "Tidal response of rocky and ice-rich exoplanets". In: *Astronomy & Astrophysics* 630, A70. DOI: 10.1051/0004-6361/201935297.

Tobie, G., G. Choblet, and C. Sotin (2003). "Tidally heated convection: Constraints on Europa's ice shell thickness". In: *J. Geophys. Res. Planets* 108.E11, 5124. DOI: 10.1029/2003JE002099.

Tosi, N. et al. (2017). "The habitability of a stagnant-lid Earth". In: *Astronomy & Astrophysics* 605, A71. DOI: 10.1051/0004-6361/201730728.

Tyler, R. H., W. G. Henning, and C. W. Hamilton (2015). "Tidal Heating in a Magma Ocean within Jupiter's Moon Io". In: *Astrophys. J. Suppl.* 218.2, 22. DOI: 10.1088/0067-0049/218/2/22.

Tyler, R. (2014). "Comparative estimates of the heat generated by ocean tides on icy satellites in the outer Solar System". In: *Icarus* 243, pp. 358–385. DOI: https://doi.org/10.1016/j.icarus.2014.08.037.

van Hoolst, T., R.-M. Baland, and A. Trinh (2016). "The diurnal libration and interior structure of Enceladus". In: *Icarus* 277, pp. 311–318. DOI: 10.1007/s11214-007-9202-6.

van Hoolst, T. et al. (2007). "Mercury's Interior Structure, Rotation, and Tides". In: *Space Science Rev.* 132, pp. 203–227. DOI: 10.1007/s11214-007-9202-6.

Vance, S. D., K. P. Hand, and R. T. Pappalardo (2016). "Geophysical controls of chemical disequilibria in Europa". In: *Geophys. Res. Let.* 43.10, pp. 4871–4879. DOI: 10.1002/2016GL068547.

Vance, S. et al. (2021). "Distributed Geophysical Exploration of Enceladus and Other Ocean Worlds". In: *Bulletin of the AAS* 53. DOI: https://doi.org/10.3847/25c2cfeb.a07234f4.

Varshalovich, D. A., A. N. Moskalev, and V. K. Khersonskii (1988). *Quantum theory of angular momentum: irreducible tensors, spherical harmonics, vector coupling coefficients, 3nj symbols.* Singapore: World Scientific.

Verma, A. K. and J.-L. Margot (2018). "Expected precision of Europa Clipper gravity measurements". In: *Icarus* 314, pp. 35–49. DOI: 10.1016/j.icarus.2018.05.018.

Wahr, J. et al. (2009). "Modeling stresses on satellites due to nonsynchronous rotation and orbital eccentricity using gravitational potential theory". In: *Icarus* 200, pp. 188–206. DOI: 10.1016/j.icarus.2008.11.002.

Waite, J. H. et al. (2017). "Cassini finds molecular hydrogen in the Enceladus plume: Evidence for hydrothermal processes". In: *Science* 356.6334, pp. 155–159. DOI: 10.1126/science.aai8703.

Walterová, M. (2021). "Orbital and internal dynamics of terrestrial planets". PhD thesis. Charles University, Prague.

Walterová, M. and M. Běhounková (2017). "Tidal effects in differentiated viscoelastic bodies: a numerical approach". In: *Celest. Mech. Dyn. A.* 129.1-2, pp. 235–256. DOI: 10.1007/s10569-017-9772-x.

Walterová, M. and M. Běhounková (2020). "Thermal and Orbital Evolution of Low-mass Exoplanets". In: *Astrophys. J.* 900.1, 24. DOI: 10.3847/1538-4357/aba8a5.

Wilson, A. and R. R. Kerswell (2018). "Can libration maintain Enceladus's ocean?" In: *Earth Plan. Sci. Let.* 500, pp. 41–46. DOI: 10.1016/j.epsl.2018.08.012.

Wisdom, J. and Z. L. Tian (2015). "Early evolution of the Earth-Moon system with a fast-spinning Earth". In: *Icarus* 256, pp. 138–146. DOI: 10.1016/j.icarus.2015.02.025.

Wright, J. T. and G. B. Scott (2013). "Exoplanet Detection Methods". In: *Planets, Stars and Stellar Systems: Volume 3: Solar and Stellar Planetary Systems*. Ed. by T. D. Oswalt, L. M. French, and P. Kalas. Dordrecht: Springer Netherlands, pp. 489–540. DOI: 10.1007/978-94-007-5606-9_10.

Wu, P. and W. R. Peltier (1982). "Viscous gravitational relaxation". In: *Geophys. J.* 70.2, pp. 435–485. DOI: 10.1111/j.1365-246X.1982.tb04976.x.

Collection of publications P

Author's contribution to the publications

All publications in this thesis are works to which I have significantly contributed. I have taken part in the discussion and interpretation of results in all papers. For the coupled thermal-tidal evolution, I have coupled and parallelized code evaluating tidal deformation and dissipation with 3D convection code. Furthermore, I have added new ingredients, including rheological description, simple melting model, and adapted the codes for the given applications (P1, P2, P3, P4, P11). I have also contributed to code development (P6, P8, P9), where my contribution mainly lies in implementing physical and postprocessing modules. I have primarily (P1, P2, P3, P4, P5, P11) or partly (P8, P9) performed the simulations and processed the data. Computations and simulations in papers (P7, P10) were performed under my supervision by Michaela Walterová (Káňová).

List of appended publications

P1 Běhounková, M., Tobie, G., Choblet, G., Čadek, O. (2010). Coupling mantle convection and tidal dissipation: applications to Enceladus and Earth-like planets, J. Geophys. Res. 115, E09011.

P2 Běhounková, M., Tobie, G., Choblet, G., Čadek, O. (2011). Tidally induced thermal runaways on extrasolar Earths: Impact on habitability, The Astrophysical Journal 728(2), article id 89.

P3 Běhounková, M., Tobie, G., Choblet, G., Čadek, O. (2012). Tidally-induced melting events as the origin of south-pole activity on Enceladus, Icarus 219(2), 655-664.

P4 Běhounková, M., Tobie, G., Choblet, G., Čadek, O. (2013). Impact of tidal heating on the onset of convection in Enceladus's ice shell, Icarus, 226(1), 898-904.

P5 Běhounková, M., Tobie, G., Choblet, G., Čadek, O., Porco, C., Nimmo, F. (2015). Timing of water plume eruptions on Enceladus explained by interior viscosity structure, Nature Geoscience 8, 601-604.

P6 Souček, O., Hron, J., Běhounková, M., Čadek, O. (2016), Effect of the tiger stripes on the deformation of Saturn's moon Enceladus, Geophys. Res. Lett. 43, pp. 7417-7423.

P7 Walterová, M., Běhounková, M. (2017), Tidal effects in differentiated viscoelastic bodies: a numerical approach. Celestial Mechanics and Dynamical Astronomy, 129: 235-256.

P8 Běhounková, M., Souček, O., Hron, J., and Čadek, O. (2017), Plume Activity and Tidal Deformation on Enceladus Influenced by Faults and Variable Ice Shell Thickness. Astrobiology 17(9), 941-954.

P9 Souček, O., Běhounková, M., Čadek, O., Hron, J., Tobie, G. and Choblet, G. (2019), Tidal dissipation in Enceladus' uneven, fractured ice shell, Icarus 328, 218-231.

P10 Walterová, M., Běhounková, M. (2020), Thermal and orbital evolution of low-mass exoplanets, The Astrophysical Journal 900(1), No. 24.

P11 Běhounková, M., Tobie, G., Choblet, G., Kervazo, M., Melwani Daswani, M., Dumoulin, C., Vance, S.D. (2020), Tidally-induced magmatic pulses on the oceanic floor of Jupiter's moon Europa, J. Geophys. Res. 48, e2020GL090077.

P1

Coupling mantle convection and tidal dissipation: applications to Enceladus and Earth-like planets

Běhounková, M., Tobie, G., Choblet, G., Čadek, O.

Published in *J. Geophys. Res. 115*, E09011 (2010)

doi:10.1029/2009JE003564

P2

Tidally induced thermal runaways on extrasolar Earths: Impact on habitability

Běhounková, M., Tobie, G., Choblet, G., Čadek, O.

Published in *The Astrophysical Journal 728(2)*, 89 (2011)

doi:10.1088/0004-637X/728/2/89

P3

Tidally-induced melting events as the origin of south-pole activity on Enceladus

Běhounková, M., Tobie, G., Choblet, G., Čadek, O.

Published in *Icarus 219(2)*, pp. 655–664 (2012)

doi:10.1016/j.icarus.2012.03.024

P4

Impact of tidal heating on the onset of convection in Enceladus's ice shell

Běhounková, M., Tobie, G., Choblet, G., Čadek, O.

Published in *Icarus 226(1)*, pp. 898–904 (2013)

doi:10.1016/j.icarus.2013.06.033

Timing of water plume eruptions on Enceladus explained by interior viscosity structure

Běhounková, M., Tobie, G., Choblet, G., Čadek, O., Porco, C., Nimmo, F.

Published in *Nature Geoscience 8*, pp. 601–604 (2015)

doi:10.1038/ngeo2475

Effect of the tiger stripes on the deformation of Saturn's moon Enceladus

Souček, O., Hron, J., Běhounková, M., Čadek, O.

Published in *Geophys. Res. Lett. 43*, pp. 7417–7423 (2016)

doi:10.1002/2016GL069415

Tidal effects in differentiated viscoelastic bodies: a numerical approach

Walterová, M., Běhounková, M.

Published in *Celestial Mechanics and Dynamical Astronomy 129*, pp. 235-256 (2017)

doi:10.1007/s10569-017-9772-x

Plume Activity and Tidal Deformation on Enceladus Influenced by Faults and Variable Ice Shell Thickness

Běhounková, M., Souček, O., Hron, J., and Čadek, O.

Published in *Astrobiology 17(9)*, pp. 941-954 (2017)

doi:10.1089/ast.2016.1629

Tidal dissipation in Enceladus' uneven, fractured ice shell

Souček, O., Běhounková, M., Čadek, O., Hron, J., Tobie, G. and Choblet, G.

Published in *Icarus 328*, pp. 218–231 (2019)

doi:10.1016/j.icarus.2019.02.012

Thermal and orbital evolution of low-mass exoplanets

Walterová, M., Běhounková, M.

Published in *The Astrophysical Journal 900(1)*, 24 (2020)

doi:10.3847/1538-4357/aba8a5

Tidally-induced magmatic pulses on the oceanic floor of Jupiter's moon Europa

Běhounková, M., Tobie, G., Choblet, G., Kervazo, M., Melwani Daswani, M., Dumoulin, C., Vance, S.D.

Published in *J. Geophys. Res. 48*, e2020GL090077 (2021)

doi:10.1029/2020GL090077